A GLIMPSE into the Nature of Galactic Mid-IR Excesses

B. Uzpen [1], H. A. Kobulnicky [1], D. Semler [2], T. Bensby [3 4], C. Thom [5], M. R. Meade [6], B. L. Babler [6], R. Indebetouw [7], B. A. Whitney [8], C. Watson [9],

and

E. Churchwell [6]

ABSTRACT

We present new results on stellar fundamental parameters for 31 stars that exhibit a mid-IR 8 μm excess in either the Galactic Legacy Infrared Mid-Plane Survey Extraordinaire or the Mid-Course Space Experiment. We determine effective temperature and projected stellar rotational velocity by comparing stellar equivalent width ratios to high-resolution stellar models. We estimate stellar ages utilizing these effective temperatures and the evolutionary tracks from Siess et al. (2000). We use Hα equivalent width to assess the contribution from free-free emission to the excess. Using MIPS [24] measurements and stellar parameters we determine the nature of the infrared excess for 19 GLIMPSE stars. We find that four stars do not exhibit Hα emission, exhibit circumstellar dust temperatures between $\approx$200–400K, have $\frac{L_{IR}}{L_*} \sim 10^{-3}$ and are warm debris disk candidates. Seven stars exhibit Hα luminosities that imply free-free emission that can plausibly explain the infrared excess at [24]. These stars are candidate classical Be stars. The remaining eight stars exhibit Hα emission but determined Hα fluxes are insufficient to explain the infrared excesses at [24]. After the removal of the

[1]University of Wyoming, Dept. of Physics & Astronomy, Dept. 3905, Laramie, WY 82071

[2]Columbia Astrophysics Laboratory, Columbia University, 550 West 120th Street, New York, NY 10027

[3]University of Michigan, Department of Astronomy 500 Church St, Ann Arbor, MI 48109-1042

[4]European Southern Observatory, Alonso de Cordova 3107, Vitacura, Casilla 19001, Santiago Chile

[5]The University of Chicago, Department of Astronomy & Astrophysics 5640 S. Ellis Ave, Chicago, IL 60637

[6]University of Wisconsin-Madison, Dept. of Astronomy, 475 N. Charter St., Madison, WI 53706

[7]University of Virginia, Dept. of Astronomy, P.O. Box 3818, Charlottesville, VA 22903-0818

[8]Space Science Institute, 4750 Walnut St. Suite 205, Boulder, CO 80301

[9]Manchester College, Dept. of Physics, North Manchester, IN 46962

free-free component, we determine that the circumstellar parameters vary from ∼300–800 K with $\frac{L_{IR}}{L_*}$ ≈10^{-3}. We conclude that the excess in these eight stars may require the presence of a circumstellar dust component. These eight stars may be pre-main-sequence stars with transitional disks undergoing disk clearing.

Subject headings: Line: profiles — Stars: Fundamental Parameters, Emission-line, Be, Rotation, Circumstellar matter — Techniques: spectroscopic

1. Introduction

Circumstellar disks exist around stars at a wide range of ages, but the nature of these disks varies (Zuckerman 2001). Young stars form circumstellar disks through the collapse of the initial molecular cloud as a method to conserve angular momentum (Shu et al. 1987). Intermediate- and low-mass pre-main-sequence stars accrete gaseous material via their circumstellar disks as they evolve towards main-sequence stars (Waters & Waelkens 1998; Bertout 1989). Circumstellar dust disks, presumably due to planetesimal collisions, surround some main-sequence stars (Backman & Paresce 1993; Lagrange et al. 2000). Circumstellar gaseous disks that emit excesses owing to free-free emission surround other main-sequence stars (Porter & Rivinius 2003). Circumstellar disks can surround evolved giants as well (Jura 1999). By understanding the nature of the circumstellar disks, we can better understand how these disks evolve.

Intermediate mass stars (2–10 $M_\odot$) typically exhibit circumstellar disks in their pre-main-sequence phase as Herbig AeBe stars (Herbig 1960), as main-sequence stars with debris disks, (Backman & Paresce 1993), and main-sequence to late-stage main-sequence stars known as classical Be stars (Struve 1931; McSwain & Gies 2005). Herbig AeBe stars are young stars accreting circumstellar material via their disk (Strom 1972; Hillenbrand et al. 1992; Hartmann et al. 1993). Emission lines and infrared excesses evidence this accretion (Hillenbrand et al. 1992). Waters & Waelkens (1998) suggests the following as criterion for Herbig AeBe stars: (1) an emission-line A or B star, (2) an infrared excess owing to circumstellar dust, either hot or cool, and (3) luminosity class III–V. As the disk dissipates the emission lines weaken and infrared excess decreases and appears only at longer wavelengths (e.g., The et al. 1994).

Classical Be stars are typically rapidly rotating B stars with Hα emission and an IR excess from free-free emission (Gehrz et al. 1974; Balona 2000). These stars are variable in both emission-line strength and photometric colors (Dachs et al. 1988). The circumstellar disk for classical Be stars is thought to be a mechanism for mass loss unlike, Herbig AeBe

stellar disks (Balona 2000). Classical Be stars are similar to Herbig AeBe stars in that they both exhibit emission lines due to circumstellar gas (Struve 1931; Herbig 1960). The greatest distinction between Herbig AeBe stars and classical Be stars is the nature of the infrared excess with dust in the former, and thermal bremsstrahlung in the latter.

Aumann et al. (1984) reported the first detection of an infrared excess owing to dust in the Vega system, and this excess was later explained as a debris disks. To date, many debris disks have been found with *IRAS*, *Infrared Space Observatory (ISO)*, and *Spitzer Space Telescope* (*Spitzer*; Werner et al. 2004) (Backman & Paresce 1993; Spangler et al. 2001; Meyer et al. 2004). Lagrange et al. (2000) suggested a definition of debris disks using four criteria. These criteria require that the fractional infrared luminosity ($\frac{L_{IR}}{L_*}$) is small, i.e., $\frac{L_{IR}}{L_*} \leq 10^{-3}$, the mass of the gas and dust must be $< 10^{-2}$ $M_\odot$, the dust mass must be significantly greater than the gas mass, and the grain destruction time must be much less than the stellar age. Debris disks typically have $\frac{L_{IR}}{L_*}$ between $\sim 10^{-5}$ and 10^{-3} with most between 10^{-5} and 10^{-4} (Decin et al. 2003). Large fractional excess debris disks are rare; Bryden et al. (2006) found a debris disk fraction of 2±2% at 24 μm, for main-sequence field FGK stars with $\frac{L_{IR}}{L_*} \geq 10^{-4}$.

"Transition disks" are especially interesting as possible evolutionary links between the optically thick Herbig AeBe disk systems and the older optically thin debris disk systems. Transition disks may be evolved protoplanetary disks with inner holes caused by clearing of the initial gas-dominated disks from the inside out (Strom et al. 1989). These disks would be optically thin at near- and mid-IR wavelengths and optically thick in the far-IR. These sources would show weak to no accretion signatures (Sicilia-Aguilar et al. 2006b). Intermediate mass candidate transition disks have only recently been discovered (Hernández et al. 2006; Sicilia-Aguilar et al. 2006a; Hernandez et al. 2007).

By investigating the nature of the infrared excess and optical spectral features, we can distinguish between various types of circumstellar disks that persist around intermediate mass stars. In order to understand the nature of the infrared excess surrounding a star we must determine the fundamental parameters of the star. In this paper we present results of spectroscopic analysis for mid-IR excesses identified in the *Spitzer* Galactic Legacy Infrared MidPlane Survey Extraordinaire (GLIMPSE; Benjamin et al. 2003) and MidCourse Space Experiment (*MSX*; Egan et al. 2003) catalogs to determine the nature of infrared excess (Uzpen et al. 2007). In §2 we describe how we obtained new optical echelle spectroscopy. In §3 we describe our methods for determining rotational velocity. In §4 we describe our methods for determining effective temperatures. In §5 we describe Hα and Fe II λ 5317Å profiles. In §6 we describe how we estimate stellar ages through main-sequence fitting utilizing our determined fundamental parameters. In §7 we describe how all of the derived parameters

provide insight into the nature of the infrared excess, how we utilize these parameters to estimate free-free emission associated with our sources, and the evolutionary state of the circumstellar disk. In §8 we describe the individual sources.

2. Target Selection and Observations

We observed 30 of 42 sources that exhibited an 8 μm mid-IR excess in Uzpen et al. (2007), 25 of which have an excess at 8 and 20+ μm. The purpose of these observations was to identify circumstellar disk characteristics based on optical spectral features. We chose stars with both known and unknown circumstellar evolutionary state.

We conducted high-resolution, high-signal-to-noise ratio spectroscopic observations at the Magellan Telescope with the Magellan Inamori Kyocera Echelle (MIKE; Bernstein et al. 2003) double echelle spectrograph on the nights of 26–28 September 2006 and 7–8 April 2007. The spectral coverage was ∼3400–9500 Å with a resolving power of R=37,000 at 4000 Å and R=29,000 at 6500 Å measured from arc spectra. Typical stellar S/N was ∼100:1. We conducted standard data reductions in IRAF including flat fielding with a continuum lamp and wavelength calibration using a ThAr arc lamp, but no flux calibration.

We observed 13 stars to use as rotational velocity standards. Seven of these stars had projected rotational velocities determined in Royer et al. (2002a). Ten of these stars had projected rotational velocities determined in Slettebak et al. (1975). Four stars had their rotational velocities determined in both papers.

3. Rotational Velocities

The most common methods for measuring the projected rotational velocities are through the computation of the first zero of a Fourier Transform of a given line profile (Carroll 1933; Gray 1992; Royer 2005) or through the measurement of a line FWHM (Slettebak et al. 1975). The FWHM of He I λ 4471, Mg II λ 4481, and Fe I λ 4476 are shown to correlate with v sin i in Slettebak et al. (1975) and is the method we adopt to measure projected rotational velocity. However, this method is less reliable at lower rotational velocities, and the calibration of Slettebak et al. (1975) has been shown to be 10–12 % lower than measurements made using the Fourier Transform (Royer et al. 2002a). In order to improve upon existing linear relations between He I λ 4471, Mg II λ 4481, and Fe I λ 4476 we measure the FWHM of the rotationally broadened stellar models of Munari et al. (2005) at a resolving power of R=20,000 from 21,000–7,500 K.

Figure 1 shows the relationships between projected rotational velocity and the FWHM of He I λ 4471, Mg II λ 4481, and Fe I λ 4476. The He I λ 4471 line profile includes a Stark broadening component that causes a greater dispersion in the FWHM measurement. We derived the following equations for a linear least squares fit between the metallic line and the FWHM.

$$v\ sin\ i\ (km\ s^{-1}) = 54.25 \times He(FWHM) - 46.58\ (km\ s^{-1}) \quad (1)$$

$$v\ sin\ i\ (km\ s^{-1}) = 47.64 \times Mg(FWHM) + 2.01\ (km\ s^{-1}) \quad (2)$$

$$v\ sin\ i\ (km\ s^{-1}) = 57.04 \times Fe(FWHM) - 8.73\ (km\ s^{-1}) \quad (3)$$

The Mg FWHM relation is not linear below ∼40 km s^{-1} or above 300 km s^{-1}, while the Fe FWHM relation is linear at velocities ≥10 km s^{-1}. We estimate our uncertainties at 10% utilizing this method based on both the dispersion of the models from the best-fit line and measurement uncertainties in the FWHM. Table 1 lists the v sin i measurements of our target stars and rotational velocity standards and compares them with values listed in the literature when available. Our stellar rotational velocities agree with literature values within the uncertainties. When two rotational velocity indicators are present, the reported rotational velocity is the weighted mean of both measurements, and the uncertainty is the uncertainty of the mean. Figure 1*d* shows a comparison of our measurements to literature rotational values between Slettebak et al. (1975) and Royer et al. (2002a,b). Our values are more consistent with those derived from Royer et al. (2002a,b) and are 10–15% higher than those of Slettebak et al. (1975), which is consistent with results from other projected rotational velocity studies.

4. Surface Temperatures

We determined effective temperatures by comparing model helium, magnesium, iron, and calcium equivalent widths with the observed equivalent width. We utilized equivalent width measurements of He I λ 4009, He I λ 4471, Mg II λ 4481, Fe II λ 4233, and Ca I λ 4227 in Munari et al. (2005) R=20,000 models. We used the models in the range 7,000 K ≤ T_{eff} ≤ 21,000 K, with log g=4.5 for T_{eff} < 10000 K, and log g=4.0 for T_{eff} ≥ 10000 K. We used models with rotational broadening between 0 km s^{-1} and 400 km s^{-1}. The effective temperature step size varies from ΔT_{eff}=1000 K for 12,000 K < T_{eff} ≤ 21,000 K, ΔT_{eff}=500 K for 10,000 K ≤ T_{eff} < 12,000 K and ΔT_{eff}=250 K for 7,000 K ≤ T_{eff} < 10,000 K.

The equivalent width ratios of Mg II λ 4481/He I λ 4009, Mg II λ 4481/He I λ 4471, Mg II λ 4481/Fe II λ 4233, and Mg II λ 4481/Ca I λ 4227 form monotonic relations depen-

dent on both temperature and rotational velocity spanning T=21,000–7,000 K, as shown in Figure 2. The *solid* curves in Figure 2 show the best-fit functions to the EW ratio and stellar effective temperature. We chose Mg and He because these atoms are present in B and early A stars, and He strength decreases rapidly in late B stars. Fe lines start to appear in early A stars and increase in strength toward later spectral types. Ca lines increase in strength and number starting at late A stars and continuing through F stars. At rotational velocities > 150 km s^{-1} the Mg II λ 4481/He I λ 4009 and Mg II λ 4481/He I λ 4471 ratios are independent of rotational velocity and thus provide the best estimates of T_{eff}. At rotational velocities < 150 km s^{-1} the Mg II λ 4481/Ca I λ 4227 ratios are independent of rotational velocity and provide the best estimates of T_{eff}.

We determined the effective temperature utilizing one or more equivalent width ratios for our target stars and present them in Table 2. The uncertainties in effective temperatures were determined by adding in quadrature the uncertainty derived from equivalent width fitting with one-half the model step size. The later uncertainty component approximately accounts for the random uncertainty in measuring the stellar equivalent width by defining of the continuum. In general, most derived effective temperature measurements are consistent with the stellar spectral classification within uncertainties. We found several late B stars to have effective temperatures hotter than their spectral classifications would indicate. This discrepancy may be in part due to differences between observational parameters and theoretical stellar models. Under the MK system, the definition of a B8 main-sequence star requires He I λ 4471 line equal to the Mg II λ 4481 line. The observational calibration temperature for a B8 main-sequence star is 11400 K (Cox 2000). However, utilizing the MK system definition of a B8 main-sequence star and Munari et al. (2005) models we would derive a temperature of $\sim$12600 K through interpolation of the model grids. We do not present revised spectral types for the late B stars in Table 2 due to the systematic difference between optical classification criteria and theoretical models.

5. Hα & Fe II

The nature of an infrared excess can in part be determined through Hα spectroscopy. By definition, classical Be stars and Herbig AeBe stars exhibit Balmer emission lines owing to their circumstellar gaseous shell or disk. In contrast, debris disks do not exhibit any Balmer emission lines and are devoid of significant amounts of circumstellar gas (Lagrange et al. 2000). We measured the Hα equivalent width (EW) for our targets and noted the five Hα profile types in Table 3. These profile types include single-peaked emission profiles (S), double-peaked emission profiles (D), absorption profiles (A), P-Cygni emission profiles

(P), and inverse P-Cygni emission profiles (IP). For complex profiles, double-peaked emission, or P-Cygni features, we measured each of the components of the profile and took the sum. For each star, we measured the profile five times to determine the mean of the EW. Uncertainties on EW were determined through the standard deviation of the five separate EW measurements added in quadrature. We then utilized Munari et al. (2005) stellar model Hα absorption measurements to correct the Hα equivalent width for underlying absorption. This measure, EW(H$\alpha)_{corr}$, is then used for the remainder of this paper. Normalized Hα spectra are shown in Figures 3 & 4. Only one-third of the sample, ten stars, exhibit Hα absorption profiles. Of the remaining twenty stars that exhibit Hα emission, only one star exhibits single-peaked emission, one star exhibits inverse P-Cygni, and one star exhibits P-Cygni profiles. The majority of the stars that exhibit Balmer emission show a double-peaked emission profile, 17 stars. We expected this given that the majority of both classical Be and Herbig AeBe stars exhibit emission as a double-peaked profile (Porter & Rivinius 2003; Finkenzeller & Mundt 1984).

Classical Be stars exhibit metallic lines in emission, especially Fe II (Jaschek et al. 1980; Hanuschik et al. 1996). Presence or absence of Fe II is one criterion for classification of classical Be stars into subgroups (Jaschek et al. 1980). We show continuum normalized spectra near Fe II 5317 Å in Figures 5 and 6. Only four sources exhibit Fe II in emission: G027.0268+00.7224 (A0V), G229.4514+01.0145 (B9V), G321.7868+00.4102 (B8VN), and G340.0517+00.6682 (B8). Jaschek et al. (1980) Group I sources, stars with Fe II emission, are of spectral type B0-B6. These stars may be an extension to later spectral types for Group I classical Be stars. Herbig AeBe stars have also been shown to exhibit Fe I and Fe II emission, but the EW of Hα for such sources show strong emission, EW(Hα) $<$ -25 Å (Hernández et al. 2004). G340.0517+00.6682 is the only one of the sources to exhibit strong Hα emission, EW(Hα_{corr})=-39.38 Å.

6. Age Determination

Using our derived T_{eff} and trigonometric parallaxes from *Hipparcos*/Tycho, we estimated stellar ages by fitting stellar parameters to Siess et al. (2000) model tracks on an HR diagram. *Hipparcos* parallaxes were the preferred distance measures and used when available, 10 stars. In only one instance, we used Tycho parallaxes. If neither parallax was available, we used absolute visual magnitudes derived in the literature using methods such as Hβ luminosity and intrinsic Stromgren colors of luminosity classes (see Seidensticker 1989; Westin 1985; Kozok 1985). We used parallactic distances in Table 4 unless noted. We then interpolated a bolometric correction using Cox (2000) effective temperature and

bolometric corrections and our derived effective temperatures. We corrected the Tycho-2 visual magnitude for distance and extinction to derive the absolute bolometric luminosity using the distance modulus. In order to derive age estimates we required stellar bolometric magnitude and effective temperature to be within the bounds of Siess et al. (2000) Z=0.02 models. Table 4 lists the possible age ranges for the stars with sufficient measurements and compares them to other results in the literature. The age ranges we determined for the three stars that had literature ages were consistent with the literature age, falling in one of the two determined age ranges for the given star. We were able to determine the age ranges of two pre-main-sequence stars and found that the ages we estimate are consistent with their evolutionary state. Our typical age ranges are either a few Myr or 100 Myr. Figure 7 shows our derived parameters plotted with Siess et al. (2000) Z=0.02 stellar models. The majority of our stars are consistent with 3–5 $M_{\odot}$ stellar models. Most of our stars are above the main-sequence indicating either a late pre-main-sequence or late main-sequence stellar age. Our results are similar to those derived in the literature but contain large uncertainties due to uncertain distances. Most stellar ages have uncertainties of order a few % of their lifetime, our age measurements typically have errors of 10 % or greater. The ages derived should be used as general age ranges.

7. Implication of Fundamental Parameters on the Nature of the Mid-IR Excess

7.1. Large Rotational Velocities

Abt et al. (2002) found that the rotational velocity distribution for B8-9.5 stars is bimodal with peaks at both 50 km s^{-1} and 250 km s^{-1}. Finkenzeller (1985) found that Herbig AeBe stars rotate at values of $100 < v \sin i < 225$ km s^{-1}. Boehm & Catala (1995) found that higher mass Herbig AeBe stars ($> 4M_{\odot}$) gain angular momentum as they approach the zero-age main-sequence. Boehm & Catala (1995) also found that zero-age main-sequence stars in the mass range $2.6M_{\odot} < M_{*} < 4.0M_{\odot}$ would rotate at 205±55 km s^{-1} and $M_{*} > 4.0M_{\odot}$ would rotate at 180±90 km s^{-1} based on pre-main-sequence projected rotational velocities. Our 20 GLIMPSE stars rotate between 25 km s^{-1} $< v \sin i <$ 375 km s^{-1} with a mean and dispersion of 209±76 km s^{-1}. The majority of our stars would fall in the mass range of 3–5 $M_{\odot}$. The mean projected rotational velocities of the GLIMPSE stars are consistent with the expected rotational velocities of late-stage pre-main-sequence approaching the main-sequence.

Classical Be stars are typically rapid rotators. Dachs et al. (1986) found a correlation between Hα emission line half-widths and projected rotational velocity for Be stars. Figure 8

plots projected rotational velocity versus Hα half-widths for our stars. We find no correlation between these two parameters for our stars. We compared the rotational velocities for our sample of 20 GLIMPSE late-B and early A stars (*dashed*), to B8–B9.5 stars from Abt et al. (2002) (*solid*) and classical Be stars from Hanuschik et al. (1996) (*dash-dot*), Figure 9. We performed a KS test by comparing our sample to both the classical Be sample and B8–B9.5 sample to determine if they could be the parent distribution. The probability that our sample could be derived from the Abt et al. (2002) sample is < 0.1 %. The probability that our sample may be derived from the Hanuschik et al. (1996) sample is 8 %. The mean projected rotational velocity and dispersion of the Abt et al. (2002) late B star sample is 148±84 km s^{-1}. The mean projected rotational velocity and dispersion of Hanuschik et al. (1996) classical Be stars is 217±17 km s^{-1}. Although the mean projected rotational velocities of our GLIMPSE stars are consistent with that of the Hanuschik et al. (1996) classical Be stars it is unlikely that our sample consists of solely Be stars. This result may imply that our sample is a mixed group of sources including both normal B stars, classical Be stars and even Herbig AeBe stars.

7.2. Infrared Colors

Using the working definition of Waters & Waelkens (1998) for Herbig AeBe stars, the only differing criterion between classical Be and Herbig AeBe stars is the nature of the infrared excess. While Herbig AeBe stars have an infrared excess due to circumstellar dust and gas, classical Be stars owe their infrared excess to free-free emission in ionized gas.

Color-color plots are often used to distinguish various types of infrared sources (e.g., Walker et al. 1989; Zhang et al. 2004). Using a color-color plot in both the near- and mid-infrared we can distinguish between sources that have an excess owing to free-free emission (and free-bound emission) and sources that have dust emission. In order to determine the contribution of free-free emission to the infrared continuum we utilize the following equations from Tucker (1975) to estimate the free-free flux. The free-free emissivity at a given frequency is

$$j_{ff}(\nu) = 5.44 \times 10^{-39} \frac{g_{ff} Z_i^2 N_e N_p}{\sqrt{T}} e^{-h\nu/kT} (erg\ cm^{-3}\ s^{-1}\ sr^{-1}\ Hz^{-1}) \quad (4)$$

where N_e and N_p are the electron and proton densities, T is the electron temperature, and g_{ff} is the Gaunt factor. We assumed an electron temperature of 15,000 K, a pure hydrogen gas, Z=1, and N_e=N_p=100 cm^{-3}. We used Gaunt factors from Figure 5 of Karzas & Latter (1961) by fitting a polynomial to wavelength. This fit is given by Equation 5 where λ is in

μm.

$$g_{ff} = 33.513 - 4.041 \times Log(\lambda) + 0.106 \times Log(\lambda)^2 + 0.001 \times Log(\lambda)^3 \quad (5)$$

In the near-infrared, the contribution of free-bound emission is not negligible. Ashok et al. (1984) found the contributions from free-free and free-bound to the total nebular emission at 2.2 μm are 63% and 37% respectively. We therefore include free-bound emission in our calculation of free-free emission. The emissivity of free-bound emission at a given frequency is

$$j^{fb}_{\lambda,n} = 1.4 \times 10^{-33} n^{-3} N_e N_p T^{-3/2} Z^4 e^{(\chi_n - h\nu)/kT} (erg\ cm^{-3}\ s^{-1}\ sr^{-1}\ Hz^{-1}) \quad (6)$$

where n is the excitation level of hydrogen, N_e is the electron density, N_p is the proton density, T is the electron temperature. We used the same values for free-bound as we did for free-free emission for electron density, proton density, and electron temperature.

We used the above equations for free-free and free-bound emission to determine the colors of stellar blackbodies that exhibit thermal bremsstrahlung emission. We simulated the free-free contribution to the stellar blackbody by adding increasing amounts of free-free (and free-bound) emission normalized at 8 μm to a B8V stellar model from Kurucz (1993). We varied the free-free contribution from 0.01% of the stellar blackbody at 8 μm to 100 times the stellar blackbody at 8 μm. Varying the electron temperature of the circumstellar component between 5,000 K and 15,000 K had a negligible effect on the broadband IR colors. We then used these colors to determine if we can distinguish between free-free emission and dust emission in color-space.

Figure 10 shows a plot of 8-24 μm vs. K-8 μm colors for the 20 GLIMPSE stars. Classical Be stars are those from Zhang et al. (2004). We utilized MSX A band and IRAS 25 μm as 8 μm and 24 μm measurements for the sources from Zhang et al. (2004, 2005) respectively. Thirty-five stars have MSX A band and IRAS 25 μm measurements. Both Be catalogs, Zhang et al. (2004, 2005), draw on Be stars from Jaschek & Egret (1982), however at least 7 of the 35 Jaschek & Egret (1982) sources have some indication in the literature that they may be Herbig Be stars rather than classical Be stars. The reddening vector is shown for A_V=5.0 by the arrow. The *solid* curve denotes a B8V main-sequence star with A_V=1.0 and increasing contribution from a free-free component at 8 μm. The solid symbols denote where the flux at 8 μm is due to 5%, 33% and 50% circumstellar contribution. The *dashed* curves denote a B8V main-sequence star with A_V=1.0 and an 800 K or 300 K blackbody circumstellar component. We added the blackbody contribution in a similar manner as the

free-free contribution. This plot shows that this color-space can distinguish between free-free and cool dust origins of the IR excesses. Hot dust is indistinguishable from free-free emission in this color space. Points to the right of the 300 K *dashed* curve can only be explained by a cool dust component. The two Hα emission GLIMPSE sources that fall outside the free-free region are G036.8722+00.6199 and G311.6185+00.2469. The three Hα absorption sources that fall in the dust only region are G014.4239-00.7657, G311.0099+00.4156, and G339.7415-00.1904. There are 14 Jaschek & Egret (1982) sources that fall in the region outside of free-free emission. They are HD 6343, HD 37318, HD 251726, HD 52721, HD 53367, HD 90177, HD 141926, BD-11 4667, HD 174571, HD 204722, HD 240010, HD 37967, HD 259431, and HD 50083. These 14 stars also contain five of the seven possible Herbig Be stars within the Jaschek & Egret (1982) sample. The two remaining possible Herbig Be stars are HD 50138 and HD 101412. These two sources show the greatest K-8 color and fall outside the plotted region. HD 50138 is also listed as a possible B[e] star (e.g., Bjorkman et al. 1998). A combination of hot dust, free-free emission, and extinction can explain the sources between the dashed curves.

7.3. Individual Stellar Free-free Emissivity

In order to distinguish between dust and ionized gas as the cause of an infrared excess, we use the Hα flux of each star to predict the gaseous circumstellar contribution to the 8 μm and 24 μm continuum, under the assumption that the Hα, free-free, and free-bound emitting volumes are coincident. We can then verify if the color-color plot in Figure 10 discriminates between infrared excesses with free-free emission and those with an excess due to cool dust. We adopt the emissivity at Hβ from Spitzer (1978),

$$4\pi j_{H\beta} = 1.24 \times 10^{-25} N_e N_p, \tag{7}$$

where N_e and N_p are the number densities of electrons and protons in cm^{-3}, respectively. We used the emissivitiy ratio of Hα to Hβ from Brocklehurst (1971) for Case B,

$$\frac{j_{H\alpha}}{j_{H\beta}} = 2.87. \tag{8}$$

Finally the flux due to free-free emission can be derived utilizing the flux at Hα and the emissivity at Hα,

$$F_{ff}(\nu) = F_{H\alpha}\frac{j_{ff}(\nu)}{j_{H\alpha}} \tag{9}$$

Where $j_{ff}(\nu)$ is the thermal bremsstrahlung emissivity at a given frequency, $j_{H\alpha}$ is the emissivity of Hα. We used an electron temperature of 10,000 K for determination of the individual stellar free-free emissivity.

We calculate the Hα flux by multiplying the absorption corrected equivalent width of the Hα line, EW(Hα)$_{corr}$, by the reddening corrected flux at R band. Unreddened R fluxes are listed in Table 3 computed from R-band magnitudes of Monet (1998) & Monet et al. (2003). We adopt extinction estimates from Uzpen et al. (2007), which may include circumstellar absorption and may be larger than true interstellar extinction. The resultant Hα flux represents a maximum free-free flux, ignoring possible variability.

As a test of our method, we used the observed Hα fluxes of H II regions from Viallefond et al. (1983), Viallefond & Goss (1986), and Viallefond et al. (1986) to predict the free-free radio fluxes. We compared our predicted radio fluxes to the measured values from Viallefond et al. (1983), Viallefond & Goss (1986), and Viallefond et al. (1986). Our derived 6 or 21 cm fluxes are a factor of $\sim$2 deficient relative to measured values. Israel & Kennicutt (1980) found typical extinctions of 1–2 magnitudes in the visual for H II regions. The Hα fluxes from Viallefond & Goss (1986) do not take into account extinction, and this may be part of the reason for the deficit. Non-thermal processes in the radio may also contribute to the radio flux. Figure 11 shows a comparison of the data for one star, G036.8722-00.4112. The thick *solid line* is the distance normalized stellar model. The thin *solid line* is the stellar model with extinction and circumstellar blackbody component from Uzpen et al. (2007). The *dash-dot* curve is the modeled free-free emission normalized using the Hα flux. The *dash-dot-dot-dot* curve is the modeled free-free emission plus the stellar component. The free-free component is not sufficient to explain the measured excess at 24 μm.

As an additional check of our method, we investigated HAeBe stars with Hα emission and infrared excesses not attributed to free-free emission. We wanted to verify that we would be able to distinguish between free-free emission and dust emission at infrared and radio wavelengths. We made an estimation of radio emission if the Hα emission were solely due to recombination of free ions for AB Aur and TY CrA. For Herbig AeBe stars, Hα emission is primarily due to accretion processes (e.g., Hillenbrand et al. 1992). We utilized effective temperatures, R magnitudes, extinctions, and projected rotational velocities from Hillenbrand et al. (1992). We used Hα equivalent width from Finkenzeller & Mundt (1984). We determined the EW(Hα)$_{corr}$ in a similar manner as our stars and undreddened the R flux to determine the Hα flux. We calculate the radio emission for AB Aur at 6 cm to be 180

mJy and TY CrA to be 110 mJy. The measured fluxes at 6 cm are < 0.2 mJy for AB Aur, and 2.03, 0.79, and 1.35 mJy for TY CrA (Skinner et al. 1993). We calculate the infrared flux at 25 μm owing to free-free emission at 2.6 mJy for AB Aur and 5.4 mJy for TY CrA. From the *IRAS* v2.0 PSC the flux at 25 μm is 48.1 Jy for AB Aur and 57.0 Jy for TY CrA (Oudmaijer et al. 1992). The infrared excess for TY CrA and AB Aur owes to dust reemission. The Hα emission for these stars is primarily owing to disk accretion processes and not free-free emission. Our models using Hα fluxes for stars with Balmer emission can distinguish the nature of the excess between free-free and dust.

We applied our free-free model to all stars with Hα emission and measured [24] flux. Table 5 gives the measured [24] flux (from Uzpen et al. 2007) for all 20 GLIMPSE stars and derived flux contribution at [24] from free-free emission for the 15 stars with emission. The excesses from seven sources are attributable to free-free emission since the removal of the free-free component results in < 3 σ excess. We designate such objects as Type I sources. The remaining 8 stars with emission and [24] measurements have an excess > 3 σ after the free-free components were removed. We designate these as Type II sources. We note that in none of our sources does the removal of the free-free component reduce the 8 μm or 24 μm flux below photospheric levels. In all cases, the correction for circumstellar free-free contributions to the mid-IR excess either reduces the 8 and 24 μm measurements to the photospheric levels or leaves a significant excess at these bands.

7.4. Variability

Both classical Be and Herbig AeBe stars exhibit variability at Hα (Dachs et al. 1988; Waters & Waelkens 1998). Our sources may also be variable at Hα and that may explain some of the Type II stars that exhibit an excess > 3.0 σ at [8.0] and [24] when the free-free component is removed. In order to assess Hα variability among this sample, we have investigated Hα profile variations for five northern stars, G011.2691+00.4208, G036.8722-00.4112 and G047.3677+00.6199, G047.4523+00.5132, and G051.6491-00.1182. The remaining five Type II stars that fall in the region of color-color space that may be caused by free-free emission and have a significant excess at 24 μm after the free-free component is removed are in the southern hemisphere and not observable from WIRO (G300.0992-00.0627, G305.4232-00.8229, G307.9784-00.7148, G314.3136-00.6977, and G340.0517+00.6687). We obtained optical spectroscopy of all stars with the WIRO-Spec instrument on the Wyoming InfaRed Observatory (WIRO) on the nights of 2005 August 14 and 15 using the 1435 l/mm volume-phase holographic grating in first order. This instrument is an integral field unit spectrograph consisting of 293 densely packed fibers in a 19×20 configuration with each fiber projecting

to 1″ on the sky. This grating provides a dispersion of 0.7 Å/pixel, a spectral resolution of 1.4 Å, and wavelength coverage of ∼1400 Å from ∼5750-7150 Å. Standard reduction techniques were utilized, including flat fielding using a continuum lamp and wavelength calibration using a CuAr arc lamp, but no flux calibration was performed. We achieved a typical signal-to-noise of 100:1 per pixel.

We also obtained optical spectroscopy using the WIRO-Longslit spectrograph on the nights of 2006 September 13 and 14. The WIRO-Longslit is a low-resolution spectrograph with a dispersion of 1.1 Å/pixel, a resolution of 2.6 Å using a 2″ slit width, and covers $\sim 4400 - 6700$ Å when using the 600 l/mm grating in second order. We used a GG455 blocking filter to remove third order contamination. We performed the same reduction procedures for the longslit data as WIRO-Spec data, and the signal-to-noise was similar.

G011.2691+00.4208, G036.8722-00.4112, G051.6491-00.1182 displayed a double-peaked emission profile all three nights. G047.4523+00.5132 exhibited absorption all three nights. G047.3677+00.6199 displayed a double-peaked emission profile on the nights of 2005 August 15, and 2006 September 27. However, on the night of 2006 September 13 the star exhibited a single-peaked emission profile. The EW(Hα)$_{corr}$ changed ∼25% and may be due to Hα variability. A variation in Hα may result in a lower than expected calculation of the free-free emission. We estimated at what level the Hα EW must vary to account for the excess at [24]. We find the EW(Hα)$_{corr}$ must double for the free-free emission to explain the excess at [24]. It is interesting to note that even if the EW(Hα)$_{corr}$ were a factor of two larger the excess is still significant at [8.0] even after removal of the free-free component.

For the five Type II stars in the southern hemisphere, we are unable to verify any variation. The Hα variability combined with the non-contemporaneous nature of the Hα and IR data, may lead us to over- or under-estimate the circumstellar free-free contribution to the [8.0] and [24] bands. If the circumstellar free-free contribution is underestimated, we expect to see a residual IR excess. The eight Type II sources may be examples of this effect. However, we find no instances of the converse, i.e. sources where the Hα emission leads to over-estimates of the circumstellar free-free contribution, thereby creating a deficit of [8.0] or [24]. We find that these five sources need to exhibit Hα equivalent width variation at two or three times the measured level to explain the excess as owing to free-free emission. Optical thickness may also play a role in decreasing the expected free-free emission. The optical depth would have to increase the Hα equivalent width a factor of two or three to explain the excess.

We also find that weak warm dust excesses may be present in stars that fall in the same region of color-color space as classical Be stars and Type I objects. G047.4523+00.5132 shows no evidence of Hα variation or emission, shows a significant excess at [24] and falls

in the region of color-color space similar to objects emitting free-free emission. Utilizing the color-color plot as a first order discriminate is useful but may not be the only parameter necessary to determine the nature of the excess.

7.5. Disk Clearing

Table 6 lists the derived circumstellar parameters for the eight Type II stars with the free-free emission component removed. Circumstellar disk temperature and fractional infrared luminosity were determined in the same manner as Uzpen et al. (2007). Table 6 also lists the derived circumstellar parameters for the four non-emission line stars, hereafter referred to as Type III. We list the circumstellar disk parameters from Uzpen et al. (2007) for the five MSX stars with $\lambda > 20$ μm observations. We correlated derived circumstellar parameters with stellar parameters to provide insight into the nature of the excess. Figure 12 shows circumstellar disk temperature and stellar effective temperature versus EW(Hα)$_{corr}$. We found a significant inverse-correlation between circumstellar disk temperature and EW(Hα)$_{corr}$ for Type II stars. The correlation coefficient of -0.84 for the eight Type II sources means < 1 % probability of obtaining such a high degree of correlation by chance. Such a correlation is expected if the Hα emission is due to a gaseous circumstellar disk undergoing a clearing of the inner disk. If the circumstellar disk were due to free-free emission, we would expect the strength of Hα equivalent width to be correlated with stellar effective temperature. The hotter stars would be more efficient at ionizing their circumstellar material when compared to cooler stars and exhibit a larger excess (Gehrz et al. 1974). We find no such correlation between stellar temperature and Hα equivalent width for Type I, Type II or Type III stars, see Figure 12.

Using our age estimates we investigated whether there is a correlation between EW(Hα)$_{corr}$, age, and $\frac{L_{IR}}{L_*}$ in Figure 13. Omitting the four pre-main-sequence stars from MSX, we used the eight Type II stars, but only five of the eight have age estimates. We plotted the younger age for Type II stars, when available. Using the five Type II sources and the one Type III source with an age, we find that age is strongly correlated with Hα equivalent width with a correlation coefficient of 0.97 indicating $< 1\%$ probability of obtaining such a high probability by chance. Using the older age when available, there is no correlation between EW(Hα)$_{corr}$ and age. Manoj et al. (2006) found that Hα line strength decreases as Herbig AeBe stars age. If our stars are part of the evolved tail to Herbig AeBe stars we would expect to see a correlation between EW(Hα)$_{corr}$ and age.

The correlation between disk temperature with Hα equivalent width, indicating possible disk clearing, and the lack of significant excess at [24] due to free-free emission, implies that

the Type II stars are not classical Be stars. We indicate our circumstellar disk classification in Table 6. Four of our *MSX* stars with mid-IR excesses are well studied in the literature and have well-known circumstellar disk characteristics. These four stars are either pre-main-sequence Herbig AeBe stars (H) or T-Tauri stars (TT). Five of the *MSX* stars do not have a confirmed excess at $\lambda > 20$ μm and thus, we do not classify their possible circumstellar disk. One *MSX* star, G229.4514+01.0145, has too many conflicting properties to distinguish between a Herbig AeBe star and classical Be star (B) at this time, see §8. Two of the Type II stars exhibit excesses consistent with terrestrial, ∼300–400 K, temperature circumstellar disks and do not fall in a region of color-color space permissible for free-free emission. These two are almost certainly transition disks (T). One of the Type II stars exhibits an excess consistent with terrestrial temperature circumstellar disks but falls in a region of color-color space indistinguishable from free-free emission. Five of the Type II stars indicate excesses consistent with hot circumstellar excesses > 500 K and at least one of these stars is variable. If these sources are transition disks, they may be less evolved than the cooler transition disks. They may fall in a similar region of color-color space as excesses owing to free-free emission due to the excess extending to shorter wavelengths. The four Type III sources do not exhibit any emission characteristics, have circumstellar disk temperatures and fractional infrared luminosities consistent with debris disks, and are candidates for massive debris disks (D). The seven Type I sources have their excesses explained as free-free emission. Type I stars are most likely classical Be stars (Be). Each object is discussed in the following section.

8. Individual Objects

HD 163296 (G007.2369+01.4894)-A1V- This star has been studied numerous times for both stellar parameters and circumstellar disk evolution. This Herbig Ae (HAe) star is only 122^{+17}_{-13} pc distant. Rotational velocities for this source are consistent in the literature, Finkenzeller (1985) derived a rotational velocity of 120^{+20}_{-30} km s^{-1}, Halbedel (1996) derived a rotational velocity of 120 km s^{-1}, Mora et al. (2001) derived a velocity of 130±6 km s^{-1}, all consistent with our calculated value of 145±15 km s^{-1}. Stellar fundamental parameters were calculated to be T_{eff}=9200±270K, M_{Bol}=0.48±0.10 from Cidale et al. (2001), and T_{eff}=9475K, M_*=2.4$M_\odot$, and 5 Myr old from Mannings & Sargent (1997). The stellar age of this star varies in the literature but is 4-6 Myr with Hα equivalent width varying between -12 – -17 Å (Kessler-Silacci et al. 2006). Pogodin (1994) found this star to exhibit rapid Hα variability. Our derived T_{eff} of 10350±230 K is hotter than literature values. Our measured Hα equivalent width is in emission but greater than the values in the literature. This star is known to vary, and this may explain the difference between our measured values and those in literature. Spectral types for this star vary between A0-A7 confirming a range of stellar

temperatures for this star (Finkenzeller 1985; Kessler-Silacci et al. 2006). Our measured parameters are consistent with the pre-main-sequence nature of this star.

HD 167905 (G008.3752-03.6697)-F3V- We classify this star as a T-Tauri based on large $\frac{L_{IR}}{L_*}$, weak Hα emission with a P-Cygni profile, low effective stellar temperature, and low rotational velocity.

HD 161643 (G009.4973+05.2441)-A7V- We do not have enough data to propose an evolutionary status for this star. This star is a spectroscopic binary, and this explain its unusual Hα absorption profile. The secondary star of this binary is $\sim$3 magnitudes fainter at V in the *Hipparcos* catalog. Longer wavelength confirmation of the excess is needed. Confirmation of the excess at small $\frac{L_{IR}}{L_*}$ would indicate a debris disk.

HD 165854 (G011.2691+00.4208)-B9V- This star is classified as a Be star. Halbedel (1996) found the rotational velocity to be 250$\pm$10 km s^{-1} and Yudin (2001) found it to be 242$\pm$10 km s^{-1}. These values are slightly greater than our derived values of 220$\pm$15 km s^{-1}. Yudin (2001) also found there to be no $V-L$ excess and no V band polarization. We find a weak double-peaked Hα profile. The excess for this star can be explained as owing to free-free emission.

HD 168246 (G014.4239–00.7657)-B8- This star does not exhibit Hα emission and has an intermediate value of projected rotational velocity, 165$\pm$ 10 km s^{-1}. $\frac{L_{IR}}{L_*}$ for this star is higher than typical for debris disks, 0.013. The circumstellar material is located at a large distance for this star, $\sim$ 75 AU. Given the lower temperature derived for this disk, this star may be a transitional disk at the end of its clearing phase. However, without any indication of a gaseous disk we designate it as a debris disk candidate.

HD 171149 (G025.6122+01.3020)-B9V- Abt & Morrell (1995) derived a rotational velocity of 280 km s^{-1} while Royer et al. (2002b) found the rotational velocity to be 301+ km s^{-1}. Our derived value of 290$\pm$20 km s^{-1} is consistent with both prior measurements. We find the Hα profile in absorption. Additional longer wavelength observations are needed to classify this star. The Hα profile needs to be studied for variability and emission. Longer wavelength infrared/radio measurements are needed to confirm the excess. With additional measurements optical and infrared/radio measurements it will be possible to distinguish between an excess due to a classical Be star, debris disk, or false excess.

HD 172030 (G027.0268+00.7224)-A0V- This star exhibits a double-peaked Hα emission profile and Fe II emission. The excess for this source is due to free-free emission. It is interesting to note that this star has a low projected rotational velocity, 25$\pm$5 km s^{-1}, which isn't typical for classical Be stars.

... (G036.8722–00.4112)-B8V- This star exhibits double-peaked Hα emission. Disk temperatures and $\frac{L_{IR}}{L_*}$ are similar, but slightly higher, than debris disks. This star falls in the region of 8-24 versus K-8 color space not explainable by free-free emission. Given that this star exhibits emission and has disk properties slightly higher than debris disks we classify this star as having a transitional disk. The possible ages for this star are widely variant, similar to either a late-stage pre-main-sequence star or late-stage main-sequence star. Given the nature of the excess and the large difference between the possible ages we adopt an age range of 6.11-6.32 Log yr.

HD 180398 (G047.3677+00.6199)-B8Ve- This star has been studied as a classical Be star (Jaschek & Jaschek 1992). Our Hα profile shows the same shape as Jaschek & Jaschek (1992). It is also shown to be a variable (Hamdy et al. 1991), consistent with our measurements. The derived disk temperature for this source is one of the highest, as is its Hα equivalent width. This star may have a transitional circumstellar disk or be a classical Be star. The age of this star is somewhere between a late-stage pre-main-sequence star and an early-stage main-sequence star. This age is consistent with a transitional nature disk. This star did fall in color-color space explainable by free-free emission. We adopt a transitional disk as the cause of the infrared excess.

HD 231033 (G047.4523+00.5132)-A0V- This is one of the few stars that exhibits Hα absorption. Disk temperatures and $\frac{L_{IR}}{L_*}$ are similar, but slightly higher, than debris disks. Since this star does not exhibit emission and we classify the circumstellar disk as a massive debris disk. The age for this star is consistent with a main-sequence or late-stage main-sequence star, which agrees with its circumstellar disk classification. The large uncertainty in age is due to the large uncertainties associated with the Tycho parallactic measurement.

HD 183035 (G051.6491-00.1182)-A0V- The Hα profile is nearly filled in and barely exhibits a double-peaked profile. This star falls in a region of color-color space explainable by free-free and has an excess consistent with such a source.

HD 182293 (G054.5163+02.4470)-K1IV- Although listed as a K1IV in Wright et al. (2003), our spectra indicate a spectral type of II-III. We omit further analysis of this source due to its evolved nature.

HD 58647 (G229.4514+01.0143)-B9V- There is a disparity of measured projected rotational velocity for this star, Grady et al. (1996) found it to be 280 km s^{-1}, as did Manoj et al. (2002). However, Mora et al. (2001) found the projected rotational velocity to be 118$\pm$4 km s^{-1}. Historically this star has been classified as a Herbig Ae/Be star, but in Manoj et al. (2002) they conclude that this star is a classical Be star based on the low fractional infrared luminosity. Monnier et al. (2005) studied the near-IR and disk properties of this source.

They measured a stellar luminosity of 295±50 $L_{\odot}$, and found a very low fractional infrared luminosity when compared to other Herbig Ae/Be stars. Vink et al. (2002) found that polarization for this star does not agree with that of classical Be stars but exhibits similar properties to HAe stars in the (Q,U) plane. They also measured the Hα equivalent width to be -8.6 Å which is consistent with our measurement of -7.82±0.45 Å assuming they have similar errors. HD 58647 may be a more evolved form of Herbig AeBe star consistent with its low fractional infrared luminosity or a classical Be star.

HD 72106 (G257.6236+00.2459)-A0IV- This is a visual double star with a separation of 0.8 arcseconds (Vieira et al. 2003). Vieira et al. (2003) conclude that the secondary of this system exhibits the infrared excess, Hα emission and is an evolved HAeBe star. The mid-IR spectra of this source exhibits similar features of solar system comets also indicating the evolved nature of a Herbig AeBe star (Schütz et al. 2005). Wade et al. (2005) measured the magnetic field of both the primary and secondary of this system and found the primary to exhibit a strong magnetic field. They argue that the primary may be a progenitor to the Ap/Bp stars. Our spectra is only of the primary star.

HD 73461 (G265.5536-03.9951)-A5V&A6/8V- This is a known wide visual binary (Brosche & Sinachopoulos 1989). We have spectra of both the primary and secondary. Neither source exhibits Hα emission. Longer wavelength confirmation of the excess is necessary to determine the nature of the circumstellar disk and confirm it. Assuming the binary system is coeval the stellar parameters constrain the primary to 2.2±0.2 $M_{\odot}$ and secondary to 2.0±0.2 $M_{\odot}$ with an age of 6.81-6.83 Log yr.

HD 74534 (G269.5873-05.8882)-G0V- Cutispoto et al. (2002) detect Ca II λ K emission. We do not detect this in our spectra. Cutispoto et al. (2003) derived a mass of 2 $M_{\odot}$, an age of < 2 Gyr, and a projected rotational velocity of 17 km s^{-1}. They find this star to be an evolved giant. We also find this star to be an evolved giant based on our spectra. Our derived projected rotational velocity of 10±5 km s^{-1} is the lowest determined for our sample. Our decreased reliability of rotational velocity at lower velocities is responsible for our discrepant results. We do not derive additional parameters for this source due to its evolved nature.

... (G299.1677–00.3922)-B8- This star exhibits a similar Hα profile as HD 172030. This star also exhibits a large fraction of its excess at [24] due to free-free emission. We classify the excess as arising from free-free emission.

HD 107609 (G299.7090–00.9704)-B8/9IV- Similar to HD 172030 and G299.1677–00.3922 this star exhibits a large fraction of the excess at [24] as free-free emission and this is the likely cause of the excess.

... (G300.0992-00.0627)-A1- This star was tentatively associated with an X-ray source from the *Uhuru* Satellite (Gursky 1972). Investigating the *Rosat* Faint Source Catalog we found the X-ray source to be 580″ away with a positional error of only 31″ (Voges et al. 2000). This source is therefore, not associated with the detected X-ray emitter. This star does exhibit a strong double-peaked Hα emission. Circumstellar disk parameters indicate a disk temperature between that of Herbig AeBe stars and those of debris disks. This excess is due to a transitional circumstellar disk and may be an early form of transitional disk.

HD 114757 (G305.4232-00.8209)-B6/8V(E)- Seidensticker (1989) derived M_V= -1.89±0.44, A_V=1.11±0.13, and distance modulus of 10.03±0.46. Hα exhibits a double-peaked emission line profile. This star exhibits a warm circumstellar disk temperature and moderate $\frac{L_{IR}}{L_*}$. Stellar age estimates indicate either an early pre-main-sequence star or a middle/late-stage main-sequence star. Free-free emission is not sufficient to explain the large excess at [24] although this source falls in color-color space that may be explained by free-free emission. We classify this source as a transitional disk object and adopt the younger stellar age of 5.88 Log yr.

HD 118094 (G307.9784-00.7148)-B8V(N)- Levenhagen & Leister (2004) derived the fundamental parameters for this star, which they list as a Be star. They found v sin i=239±30 km s^{-1}, T_{eff}=13500±550 K, Log g=3.90±0.15, Log Age=8.03±0.04 yr, Log $L_{\odot}$=2.59±0.08, and $M_{\odot}$=4.2±0.2. Our derived values of projected rotational velocity, 240±20 km s^{-1}, and temperature, 13220±520 K, are in agreement with their derived values. Our ages are somewhat discrepant. We determine this star to either be a young pre-main-sequence object or a late-stage main-sequence star, Log Age=6.00-6.30 or 7.66-8.03 yr. Even utilizing their derived parameters and the Siess et al. (2000) models we can not rule out the possibility of a ∼1 Myr star. The Hα profile indicates a highly asymmetric double-peaked emission. Based on these stellar parameters and the possibility of a few Myr age, which we adopt, we classify this excess owing to a transitional disk.

HD 121195 (G310.5420+00.4120)-B8IV(N)- Westin (1985) derived M_V=-2.953, distance=1945 pc, and T_{eff}=12940 K for this star. The derived effective temperature is in agreement with our derived effective temperature of 12430±510 K. We determined an age of ∼ 5.30 Log years utilizing Westin (1985) visual magnitude, which may not be realistic given the optical brightness. At such an age this star would be embedded and undergo substantial extinction. We find no evidence of this. The Hα profile exhibits a weak double-peaked Hα emission profile. This source exhibits an excess consistent with free-free emission.

HD 121808 (G311.0099+00.4156)-A3IV- This star exhibits a Hα absorption profile. Circumstellar disk parameters are consistent with a warm, massive debris disk.

HD 122620 (G311.6185+00.2469)-B8/9IV/V- Westin (1985) derived M_V=-0.613, distance=965 pc, T_{eff}=11190 K, and Log Age=8.275 yr. Our derived effective temperature of 10540±255 K is lower. Our age estimates are 6.08-6.18 and 8.16-8.18 Log yr. The older age is consistent with the literature but inconsistent with the nature of the excess. The free-free component of the [24] excess is one of the smallest of the sample. The circumstellar disk parameters are consistent with a warm massive debris disk. The weak double-peaked Hα emission profile contradicts a debris disk nature for this source. We classify this source as a transitional circumstellar disk and adopt the younger stellar age.

HD 126578 (G314.3136-00.6977)-A1IV- This star exhibits the weakest Hα emission profile. The circumstellar parameters indicate a debris disk but the weak emission precludes such classification. This star falls in a region of color-color space where excesses due to free-free emission are permissible. This star may be at the end of its transitional disk phase.

HD 135354 (G321.7868+00.4102)-B8VN- Kozok (1985) derived distances, absolute visual magnitudes, reddening for Be stars including this star. The absolute visual magnitude for this star is -1.18 at a distance of 1.01 kpc. Utilizing these parameters a stellar age range of 5.83-6.12 and 8.01-8.13 Log yr were determined. The excess for this source is consistent with free-free emission.

HD 151228 (G339.4392-00.7791)-A0/1 IV/V- The excess at [8.0] is not confirmed for this star at [24]. This source is a false mid-IR excess source.

HD 151017 (G339.7415–00.1904)-A0- This star exhibits an Hα absorption profile. Circumstellar disk parameters are consistent with a warm, massive debris disk.

HD150625 (G340.0517+00.6687)-B8- Kozok (1985) derived an absolute visual magnitude of -1.87 and a distance of 0.83 kpc. Using these parameters we constrain stellar ages to 5.62–5.85 and 7.81–7.90 Log yr. This star exhibits a strong Hα profile but the Hα flux is insufficient to explain the excess at [24]. Circumstellar parameters indicate this star has one of the hottest and most massive disks. This star exhibits Fe II emission. This star is either at the end of its Herbig AeBe phase or the beginning of its transitional disk phase and we adopt the younger stellar age range.

HD 152404 (G347.3777+04.2010)-F5V- This star is a spectroscopic binary in the Upper Centarus-Lupus with an orbital period of 13.6 days (Manset et al. 2005). This star is $\sim$ 17 Myr old and classified as F5V (Chen et al. 2005). This star has a strong excess ratio given its age and may be a long lived primordial disk (Siegler et al. 2007). Our projected rotational velocity for the two stars is 15±5 km s^{-1} consistent with 18.5±1.0 km s^{-1} from (Alencar et al. 2003). Due to the nature of this binary source we do not derive effective temperature since our method of deriving temperature does not extend to spectroscopic

binaries of similar mass. The Hα profile indicates an unusual double peaked inverse P-Cygni profile. This may indicate circumstellar accretion.

9. Conclusion

We obtained high-resolution optical spectroscopy for 31 stars of spectral type B8 or later exhibiting 8 μm mid-IR excesses in the GLIMPSE and *MSX* catalogs. We measured stellar effective temperatures for 28 stars and projected rotational velocities and Hα equivalent width for 30 stars. The projected rotational velocities of our 20 GLIMPSE stars lie between 25 and 370 km s^{-1} with a mean and dispersion of 209$\pm$76 km s^{-1}. This is larger than the mean projected rotational velocity of 148$\pm$84 km s^{-1} for late B field stars (Abt et al. 2002) but consistent with the mean projected rotational velocities of 217$\pm$17 km s^{-1} for classical Be stars from Hanuschik et al. (1996). The mean projected rotational velocity of our sample is also consistent with the mean main-sequence projected rotational value of 205$\pm$55 km s^{-1} for 2.5–4$M_{\odot}$ stars determined via spin-up of pre-main-sequence stars from Boehm & Catala (1995). We used derived stellar parameters and distances to estimate stellar ages ranging from $\sim$1 Myr to 100 Myr for 16 stars (9 of the 20 GLIMPSE stars). Twenty of the 31 stars (16 of the 20 GLIMPSE stars) exhibit Hα emission, consistent with characteristics of massive pre-main-sequence stars (i.e., Herbig AeBe stars) or classical Be stars. Hα equivalent widths range between -39.38 Å (characteristic of classical Be stars or Herbig AeBe stars) and 9.41 Å (main-sequence B and A stars), suggesting a variety of origins in a sample of objects spanning a range of stellar evolutionary states.

For 16 of the 20 GLIMPSE stars showing Hα emission, we use the Hα flux to estimate the expected contribution of free-free (and free-bound) emission to the mid-IR excesses. In seven out of the 16 cases, the expected IR excess can fully account for the observed infrared excess (Type I). We did not confirm the 8 μm excess at 24 μm in one case. In the remaining eight cases, Type II sources, the expected contribution from free-free emission cannot account for all of the observed IR excess, implying that either 1) the circumstellar excess is time-variable and the non-contemporaneous nature of Hα and mid-IR data render this estimate invalid, or 2) there is a dust component to the IR excess. The lack of evidence for Hα variability for the majority of our sources, combined with the fact that in no instance does the Hα *over predict* the IR excess component, makes the first scenario unlikely. We conclude that the second scenario, the presence of a circumstellar dust component, is most probable. Therefore, the eight Type II sources with IR excesses requiring a dust component are likely to be young main-sequence or near main-sequence objects harboring warm (300–800 K) circumstellar dust. The nominal fractional excess luminosities for these eight sources after

removal of the free-free component is $\sim 10^{-3}$. Five of these eight sources show a correlation between estimated age and Hα EW consistent with a progression of disk clearing with time. Such characteristics make these stars candidates for being "transition disk" or "post-HAeBe" systems containing rare dissipating primordial gas and dust disks. The four systems lacking Hα emission have disk temperatures of 200–400 K and fractional infrared luminosities of 10^{-2}–10^{-3}. These characteristics make them candidates for dusty debris disk systems.

We show that K-8, 8-24 color-color diagrams are a useful tool to distinguish cool (T_d < 300 K) dusty mid-IR excess objects from hot ($T_d > 500$ K) dusty or free-free mid-IR excesses. Such diagrams reveal that additional information beyond near/mid-IR colors is necessary to distinguish hot dusty from free-free excesses. This diagram also reveals that some stars cataloged as classical Be stars may in fact be late-stage pre-main-sequence stars containing circumstellar dust.

We would like to thank Mary Putnam and Sally Oey for their assistance in obtaining the Magellan observations. B.U. acknowledges support from a NASA Graduate Student Researchers Program fellowship, grant NNX06AI28H. This research has made use of the SIMBAD database, operated at CDS, Strasbourg, France. This publication makes use of data products from the Two Micron All Sky Survey, which is a joint project of the University of Massachusetts and the Infrared Processing and Analysis Center/California Institute of Technology, funded by the National Aeronautics and Space Administration and the National Science Foundation.

Table 1. Projected Rotational Velocities

Target	HD	Spec.	$v \sin i$ km s^{-1}	Lines Used	$v \sin i$ (Literature) km s^{-1}	References
G007.2369+01.4894	163296	A1V	145±15	M		
G008.3752-03.6697	167905	F3V	35±5	F		
G009.4973+05.2441	161643	A7V	140±15	M		
G011.2691+00.4208	165854	B9V	220±15	H,M	250±10, 242±10	(1), (2)
G014.4239–00.7657	165854	B8	165±10	H,M		
G025.6122+01.3020	171149	B9V	290±20	H,M	280, 301	(3), (4)
G027.0268+00.7224	172030	A0V	25±5	M		
G036.8722–00.4112	...	B8V	295±20	H,M		
G047.3677+00.6199	180398	B8Ve	310±25	H,M		
G047.4523+00.5132	231033	A0V	150±10	H,M		
G051.6491–00.1182	183035	A0V	270±20	H,M		
G229.4514+01.0145	58647	B9V	295±20	H,M	118, 280	(5), (6)
G257.6236+00.2459	72106	A0IV	240±25	M		
G265.5536-03.9951-Primary	73461	A5V	25±5	F		
G265.5536-03.9951-Secondary	...	A6/8V	40±5	F		
G269.5873-05.8882	74534	G0V	10±5	F	17	(7)
G299.1677-00.3922	...	B8	130±10	H,M		
G299.7090-00.9704	107609	B8/9IV	175±15	H,M		
G300.0992-00.0627	...	A1	255±20	H,M		
G305.4232-00.8229	114757	B6/8V(E)	230±20	H,M		
G307.9784-00.7148	118094	B8V(N)	240±20	H,M		
G310.5420+00.4120	121195	B8IV(N)	270±20	H,M		
G311.0099+00.4156	121808	A3IV	235±25	M		
G311.6185+00.2469	122620	B8/9 IV/V	265±20	H,M		
G314.3136-00.6977	126578	A1IV	205±20	M		
G321.7868+00.4102	135354	B8VN	230±20	H,M		
G339.4392–00.7791	151228	A0/1 IV/V	40±5	M		
G339.7415–00.1904	151017	A0	240±15	H,M		
G340.0517+00.6687	150625	B8	230±15	H,M		
G347.3777+04.2010	152404	F5V	15±5	F		
	22252	B8V	255±20	M	249	(8)
	48757	A0V	30±5	M	27	(8)
	50853	A0V	205±20	M	195	(8)
	181454	B8V	80±10	H,M	75	(9)
	100673	B9Ve	150±15	M	160,125	(8), (9)
	97277	A2IV	55±5	M	45	(9)
	83953	B6V	285±20	H,M	260	(9)
	95370	A3IV	95±10	M	86, 90	(8), (9)
	83754	B5V	190±20	H,M	150	(9)
	98718	B5Vn	325±35	H	280	(9)
	90994	B6V	105±10	H,M	80	(9)
	78045	A3V	50± 5	M	34, 25	(8), (9)
	83446	A5V	135±15	M	133, 125	(8), (9)

Note. — See Uzpen et al. (2007) for further information about GLIMPSE or MSX Catalog ID. Line profiles used to derive projected rotational velocities are M for Mg II λ 4481, H for H II λ and F for Fe I λ 4476. (1) Halbedel (1996); (2) Yudin (2001); (3) Abt & Morrell (1995); (4) Royer et al. (2002b); (5) Mora et al. (2001); (6) Grady et al. (1996); (7) Cutispoto et al. (2003); (8) Royer et al. (2002a); (9) Slettebak et al. (1975)

Table 2. Effective Temperatures

ID	Spec.	T_{eff} K
(1)	(2)	(3)
G007.2369+01.4894	A1V	10350±230
G008.3752-03.6697	F3V	7260±160
G009.4973+05.2441	A7V	8320±130
G011.2691+00.4208	B9V	12350±520
G014.4239–00.7657	B8	16460±640
G025.6122+01.3020	B9V	12520±510
G027.0268+00.7224	A0V	10510±300
G036.8722–00.4112	B8V	11740±260
G047.3677+00.6199	B8Ve	15700±600
G047.4523+00.5132	A0V	12260±510
G051.6491–00.1182	A0V	13100±530
G229.4514+01.0145	B9V	10220±390
G257.6236+00.2459	A0IV	11530±300
G265.5536-03.9951-Primary	A5V	7660±140
G265.5536-03.9951-Secondary	A6/8V	7040±170
G269.5873-05.8882[a]	G0III	...
G299.1677-00.3922	B8	16010±730
G299.7090-00.9704	B8/9IV	12520±505
G300.0992-00.0627	A1	13510±510
G305.4232-00.8229	B6/8V(E)	13520±510
G307.9784-00.7148	B8V (N)	13220±520
G310.5420+00.4120	B8IV(N)	12430±510
G311.0099+00.4156	A3IV	9800±130
G311.6185+00.2469	B8/9 IV/V	10540±255
G314.3136-00.6977	A1IV	9870±130
G321.7868+00.4102	B8V N	12340±505
G339.4392–00.7791	A0/1 IV/V	8800±150
G339.7415–00.1904	A0	12220±510
G340.0517+00.6687	B8	14080±520
G347.3777+04.2010[b]	F5V	...

Note. — (a) The indicated that this star is a giant. See §8 for further details. (b) This star is a spectroscopic binary. Equivalent width measurements vary too greatly to determine temperature. See §8 for further details.

Table 3. Hα Equivalent Width Measurements

ID	Spec. Type	Date	EW(Hα) Å	EW(Hα)$_{abs}$ Å	EW(Hα)$_{corr}$ Å	R_0 Flux erg cm^{-2} s^{-1} Å^{-1}	Hα Flux erg cm^{-2} s^{-1}	Hα Profile
(1)	(2)	(3)	(4)	(5)	(6)	(7)	(8)	(9)
G007.2369+01.4894	A1V	20060928	-26.15±0.15	...	...	1.42×10^{-11}	...	S
G008.3752-03.6697	F3V	20060928	-0.17±0.08	...	...	2.12×10^{-12}	...	P
G009.4973+05.2441	A7V	20060928	5.11±0.02	...	...	2.52×10^{-14}	...	A
G011.2691+00.4208	B9V	20060927	-4.24±0.16	9.62	-13.86±0.16	1.30×10^{-12}	1.80×10^{-11}	D
G014.4239-00.7657	B8	20060927	4.45±0.03	...	0.00	1.40×10^{-13}	...	A
G025.6122+03.3020	B9V	20060928	6.42±0.09	...	...	5.99×10^{-12}	...	A
G027.0268+00.7224	A0V	20070407	-1.97±0.43	11.89	-13.86±0.43	1.74×10^{-12}	2.41×10^{-11}	D
G036.8722-00.4112	B8V	20060927	-2.39±0.15	12.68	-15.07±0.15	1.68×10^{-12}	2.53×10^{-11}	D
G047.3677+00.6199	B9Ve	20060927	-14.08±0.24	8.39	-22.47±0.24	1.79×10^{-12}	4.02×10^{-11}	D
G047.4523+00.5132	A0V	20060927	6.49±0.02	...	0.00	5.12×10^{-13}	...	A
G051.6491-00.1182	A0V	20060928	5.76±0.15	8.65	-2.89±0.15	1.30×10^{-12}	3.76×10^{-12}	D
G229.4514+01.0145	B9V	20060926	-7.82±0.45	...	...	8.66×10^{-12}	...	D
G257.6236+00.2459	A0IV	20060926	9.41±0.06	...	...	1.03×10^{-12}	...	A
G265.5536-03.9951-Primary	A5V	20060927	4.93±0.11	...	...	7.01×10^{-13}	...	A
G265.5536-03.9951-Secondary	A6/8V	20060927	3.77±0.06	...	...	2.36×10^{-12}	...	A
G269.5873-05.8882	G0III	20060926	2.12±0.03	...	...	1.04×10^{-12}	...	A
G299.1677-00.3922	B8	20070407	-4.37±0.12	9.62	-13.99±0.12	5.51×10^{-13}	7.71×10^{-12}	D
G299.7090-00.9704	B8/9IV	20070407	-1.99±0.16	8.13	-10.12±0.16	5.36×10^{-13}	5.42×10^{-12}	D
G300.0992-00.0627	A1	20070407	-13.89±0.32	7.76	-21.65±0.32	2.41×10^{-13}	5.22×10^{-12}	D
G305.4232-00.8229	B6/8V(E)	20070407	-14.22±0.42	7.76	-21.98±0.42	7.34×10^{-13}	1.61×10^{-11}	D
G307.9784-00.7148	B8V(N)	20070407	-4.63±0.69	8.64	-13.27±0.69	1.62×10^{-12}	2.15×10^{-11}	D
G310.5420+00.4120	B8IV(N)	20070407	-0.09±0.09	9.88	-9.97±0.09	6.88×10^{-13}	6.86×10^{-12}	D
G311.0099+00.4156	A3IV	20070407	5.21±0.03	...	0.00	1.67×10^{-12}	...	A
G311.6185+00.2469	B8/9IV/V	20070407	1.96±0.23	12.86	-10.90±0.23	3.12×10^{-13}	3.40×10^{-12}	D
G314.3136-00.6977	A1IV	20070407	4.20±0.29	16.83	-12.63±0.29	9.41×10^{-13}	1.19×10^{-11}	D
G321.7686+00.4102	B8V N	20070407	-16.93±0.53	9.88	-26.81±0.53	5.88×10^{-13}	1.58×10^{-11}	D
G339.4392-00.7791	A0/1IV/V	20060927	3.28±0.76	14.48	-11.20±0.76	8.58×10^{-13}	9.61×10^{-12}	D
G339.7415-00.1904	A0	20060927	5.50±0.03	...	0.00	4.15×10^{-13}	...	A
G340.0517+00.6687	B8	20060927	-31.62±0.08	7.76	-39.38±0.03	1.17×10^{-12}	4.61×10^{-11}	D
G347.3777+04.2010	B8	20060927	-0.02±0.10	...	...	2.08×10^{-12}	...	IP

Note. — (5) Hα equivalent width of the nearest stellar model. This equivalent width was then used to determine EW(Hα)$_{corr}$ and subsequently calculate the Hα flux. (7) The reddening corrected R flux. (8) Hα flux was determined only for GLIMPSE mid-IR excess stars with 24 μm measurements and Hα emission. (9) D: double-peaked profile, A: absorption only profile, S: single emission only profile, P: P-Cygni profile, IP: inverse P-Cygni profile.

Table 4. Estimated Stellar Ages

ID	Distance pc	Adopted M_{Bol} mag	Age Derived Log Yr	Age in Literature Log Yr
(1)	(2)	(3)	(4)	(5)
G007.2369+01.4894	122^{+17}_{-13}	$-1.15^{+1.34}_{-0.34}$	6.13-6.63, 8.04-8.27	6.70[a]
G009.4973+05.2441	137^{+32}_{-22}	$1.27^{+0.40}_{-0.45}$	6.65-6.95, 8.42-8.74	...
G025.6122+01.3020	114^{+12}_{-9}	$-0.10^{+0.34}_{-0.36}$	7.09-8.09	...
G036.8722–00.4112	424^{+423}_{-142}	$-1.53^{+3.40}_{-1.68}$	6.11-6.32, 8.10-8.20	...
G047.3677+00.6199	353^{+171}_{-86}	$-2.05^{+0.78}_{-1.06}$	6.87-7.72	...
G047.4523+00.5132	909^{+91}_{-755}	$-2.00^{+4.01}_{-0.37}$	6.11-6.37, 7.58-8.19	...
G051.6491–00.1182	345^{+173}_{-87}	$-0.98^{+0.79}_{-1.03}$	6.13-8.05	...
G229.4514+01.0145	277^{+79}_{-50}	$-2.25^{+0.59}_{-0.50}$	6.09-6.43, 8.37-8.43	
G257.6236+00.2459	288^{+202}_{-84}	$-0.13^{+0.84}_{-1.26}$	6.26-6.55, 7.33-8.24	
G265.5536–03.9951-Primary[b]	139^{+39}_{-22}	$0.70^{+0.42}_{-0.49}$	6.81-6.83	...
G265.5536–03.9951-Secondary[b]	139^{+39}_{-22}	$1.85^{+0.42}_{-0.50}$	6.81-6.83	...
G305.4232–00.8229[c]	$1009^{+244}-188$	-3.05±0.45	5.88, 7.87-7.95	
G307.9784–00.7148	758^{+2272}_{-326}	$-3.04^{+1.38}_{-2.10}$	6.13-6.23, 7.66-8.03	8.03±0.04[d]
G311.6185+00.2469[e]	965	-1.13 ±0.50	6.08-6.18, 8.16-8.18	8.275[f]
G321.7868+00.4102[g]	1010	-2.09±0.51	5.83-6.12, 8.01-8.13	...
G340.0517+00.6687[g]	830	-3.14±0.14	5.62-5.85, 7.81-7.90	...
G347.3777+04.2010	...	...	...	7.23[h]

Note. — (a) (Mannings & Sargent 1997); (b) Assuming both stars to be coeval only a 2.2 and 2.0 $M_{\odot}$ binary is possible given temperature measurements. (c) Utilizing Seidensticker (1989) extinction and absolute visual magnitude measurements (d) (Levenhagen & Leister 2004) (e) Utilizing Westin (1985) absolute visual magnitude. (f) Westin (1985); (g) Utilizing Kozok (1985); (h) Chen et al. (2005)

Table 5. Free-Free Contribution to the 24 μm Excess

ID	[24] Flux mJy	[24] error[a] mJy	Excess flux at [24] mJy	Free-free component mJy	% free-free	σ excess	Excess Type
(1)	(2)	(3)	(4)	(5)	(6)	(7)	(8)
G011.2691+00.4208	18.4	2.7	11.0	5.2	47±25%	2.1	I
G014.4239–00.7657	71.9	13.7	71.0	...	...	5.2	III
G027.0268+00.7224[b]	17.7	2.1	5.1	7.0	137±41%	0	I
G036.8722–00.4112	21.7	2.2	14.1	7.6	54±16%	3.0	II
G047.3677+00.6199	44.6	4.5	36.6	12.3	34±12%	5.4	II
G047.4523+00.5132	8.5	1.1	5.5	...	...	5.0	III
G051.6491–00.1182	17.8	2.8	10.7	5.5	51±26%	1.9	I
G299.1677–00.3922	7.0	0.8	4.8	5.6	117±17%	0	I
G299.7090–00.9704	5.1	0.5	2.3	1.5	65±25%	1.6	I
G300.0992–00.0627	7.3	0.8	5.6	1.6	29±14%	5.0	II
G305.4232–00.8229	16.7	1.8	13.2	4.9	37±14%	4.6	II
G307.9784–00.7148	21.5	2.2	14.0	6.3	45±16%	3.5	II
G310.5420+00.4120	5.6	0.7	2.4	1.9	79±29%	0.7	I
G311.0099+00.4156	149.4	17.9	137.5	...	...	7.7	III
G311.6185+00.2469	8.6	1.5	6.9	1.0	14±22%	3.9	II
G314.3136–00.6977	22.8	2.3	15.7	3.1	20±15%	5.5	II
G321.7868+00.4102[b]	12.6	1.3	9.9	7.5	76±13%	1.8	I
G339.4392–00.7791[c,d]	7.7	1.5	...	...	...	...	...
G339.7415–00.1904[d]	5.4	0.8	4.4	...	...	5.5	III
G340.0517+00.6687[d]	31.6	3.4	24.5	14.4	59±14%	3.0	II

Note. — (7) Determined by removing the free-free component from the [24] excess and dividing by the [24] error with 10% calibration uncertainty error added in quadrature with measured error. (a) [24] flux measurement error with 10% calibration uncertainty error added in quadrature with measured error. (b) free-free emission explains the excess at [24] but this star has an excess of 10σ at [8.0] after removal of free-free component. (c) found to have no real excess at [24]. (d) New measurement, not in (Uzpen et al. 2007).

Table 6. Circumstellar Disk Parameters

ID	K-8	8-24	Disk Temperature	$\frac{L_{IR}}{L_*}$	EW(Hα)$_{corr}$	T$_{eff}$	$v \sin i$	Evolutionary Status
	[mag]	[mag]	K		Å	K	km s^{-1}	
(1)	(2)	(3)	(4)	(5)	(6)	(7)	(8)	(9)
G007.2369+01.4894	...	...	493^{+4}_{-5}	$0.14^{+0.002}_{-0.002}$	-26.15±0.15[a]	10350±230	145±15	H
G008.3752–03.6697	...	...	566^{+7}_{-8}	$0.20^{+0.004}_{-0.004}$	-0.17±0.08[a]	7260±160	35±5	TT
G009.4973+05.2441	...	...	...	...	5.11±0.02[a]	8320±130	140±15	?
G011.2691+00.4208	0.34	1.01	...	...	-13.86±0.16	12350±520	220±15	Be
G014.4239–00.7657	0.47	4.78	191^{+5}_{-4}	$0.013^{+0.001}_{-0.001}$	4.45±0.03	16460±640	165±10	D
G025.6122+01.3020	...	...	...	...	6.42±0.09	12520±510	290±20	?
G027.0268+00.7224	0.34	0.56	...	...	-13.89±0.43	10510±300	25±5	Be
G036.8722–00.4112	0.27	1.26	427^{+16}_{-17}	$0.00072^{+0.00007}_{-0.00006}$	-15.07±0.15	11740±260	295±20	T
G047.3677+00.6199	0.93	1.24	783^{+19}_{-24}	$0.0028^{+0.0001}_{-0.0001}$	-22.47±0.24	15700±600	310±25	T/Be
G047.4523+00.5132	0.29	1.25	355^{+8}_{-8}	$0.0012^{+0.0001}_{-0.0001}$	6.49±0.02	12260±510	150±10	D
G051.6491–00.1182	0.19	1.12	...	...	-2.89±0.15	13100±530	270±20	Be
G229.4514+01.0145	...	...	579^{+4}_{-5}	$0.058^{+0.001}_{-0.001}$	-7.82±0.45[a]	10220±390	295±20	H/Be
G257.6236+00.2459	...	...	404^{+9}_{-10}	$0.12^{+0.002}_{-0.002}$	9.41±0.06[a]	11530±300	240±25	H
G265.5536–03.9951-Primary	...	...	...	...	4.93±0.11[a]	7660±140	25±5	?
G265.5536–03.9951-Secondary	...	...	...	...	3.77±0.06[a]	7040±170	40±5	?
G269.5873–05.8882	...	...	...	...	2.12±0.03[a]	...	10±5	?
G299.1677–00.3922	0.35	1.18	...	...	-13.99±0.12	16010±730	130±10	Be
G299.7090–00.9704	0.18	0.81	...	...	-10.12±0.16	12520±505	175±15	Be
G300.0992–00.0627	0.56	1.36	526^{+41}_{-32}	$0.0021^{+0.0002}_{-0.0002}$	-21.65±0.32	13510±510	255±20	T/Be
G305.4232–00.8229	0.79	1.27	675^{+37}_{-33}	$0.0038^{+0.0003}_{-0.0002}$	-21.98±0.42	13520±510	230±20	T/Be
G307.9784–00.7148	0.40	1.06	557^{+22}_{-16}	$0.00090^{+0.00007}_{-0.00008}$	-13.27±0.69	13220±520	240±20	T/Be
G310.5420+00.4120	0.25	0.70	...	...	-9.97±0.09	12430±510	270±20	Be
G311.0099+00.4156	0.37	2.79	315^{+4}_{-3}	$0.0027^{+0.0001}_{-0.0003}$	5.21±0.03	9800±130	235±25	D
G311.6185+00.2469	0.28	1.82	306^{+13}_{-6}	$0.0012^{0.0001}_{-0.0001}$	-10.90±0.23	10540±255	265±20	T
G314.3136–00.6977	0.22	1.45	328^{+11}_{-9}	$0.00096^{+0.00007}_{-0.00008}$	-12.63±0.29	9870±130	205±20	T
G321.7868+00.4102	0.77	1.25	...	...	-26.81±0.53	12340±505	230±20	Be
G339.4392–00.7791[b]	...	...	...	...	-11.20±0.76	8800±150	40±5	...
G339.7415–00.1904	0.27	1.93	311^{+6}_{-6}	$0.0010^{+0.0001}_{-0.0001}$	5.50±0.03	12220±510	240±15	D
G340.0517+00.6687	1.11	1.04	823^{+20}_{-20}	$0.015^{+0.001}_{-0.001}$	-39.38±0.08	14080±520	230±15	T/H
G347.3777+04.2010	...	...	487^{+9}_{-11}	$0.13^{+0.02}_{-0.03}$	-0.02±0.10[a]	...	15±5	TT/T

Note. — (9) H: Herbig AeBe star, TT: T-Tauri star, T: Transitional disk, D: Debris disk, Be: Excess due to free-free emission and therefore a classical Be-type star, ?: additional measurements are needed to classify the nature of the IR excess. (a) This value is EW(Hα), uncorrected for underlying stellar absorption. (b) The [8.0] excess from Uzpen et al. (2007) is not confirmed at [24].

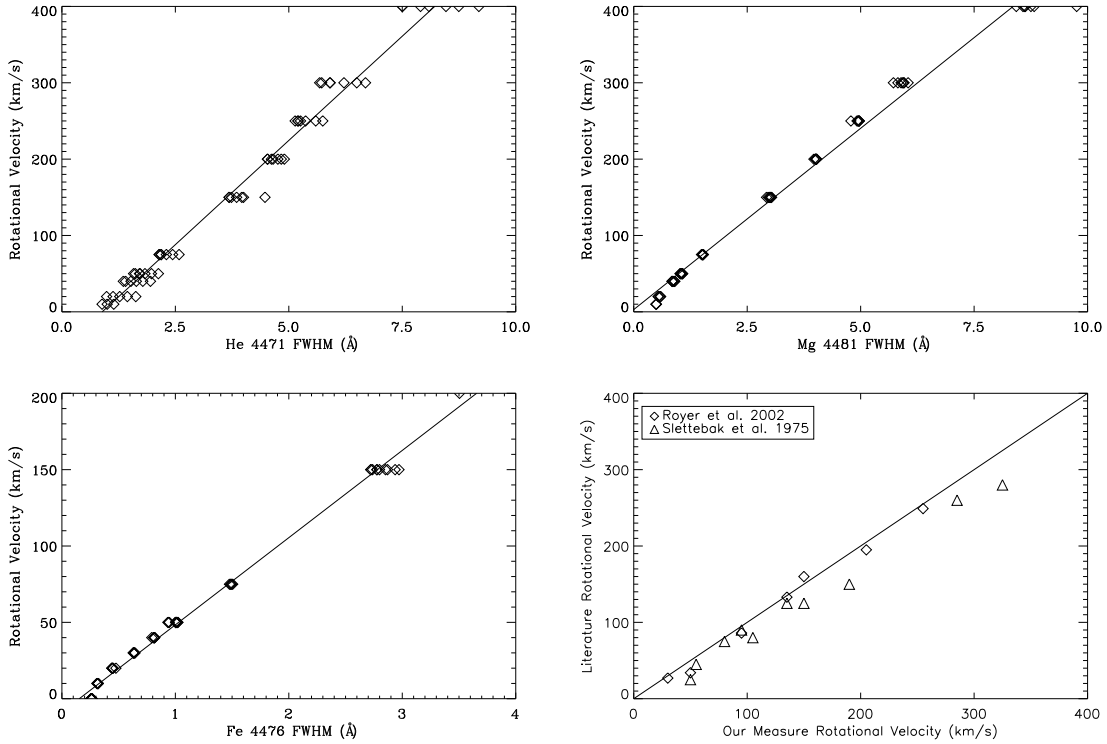

Fig. 1.— (a) The relation between He I λ 4471 FWHM and the projected rotational velocity. The He I λ 4471 line contains Stark broadening that causes a greater dispersion in the FWHM measurement. The *solid* line shows the linear least squares fit. A given velocity was measured multiple times over a range of temperatures. (b) The relation between Mg II λ 4481 FWHM and the projected rotational velocity. (c) The relation between Fe I λ 4476 FWHM and the projected rotational broadening. (d) A comparison of our projected rotational velocities to those of Royer et al. (2002a) and Slettebak et al. (1975). The *solid* line shows the 1:1 relationship in this panel. Our measurements are consistent with those of Royer et al. (2002a) but $\sim$10% larger than those of Slettebak et al. (1975), as explained in the text.

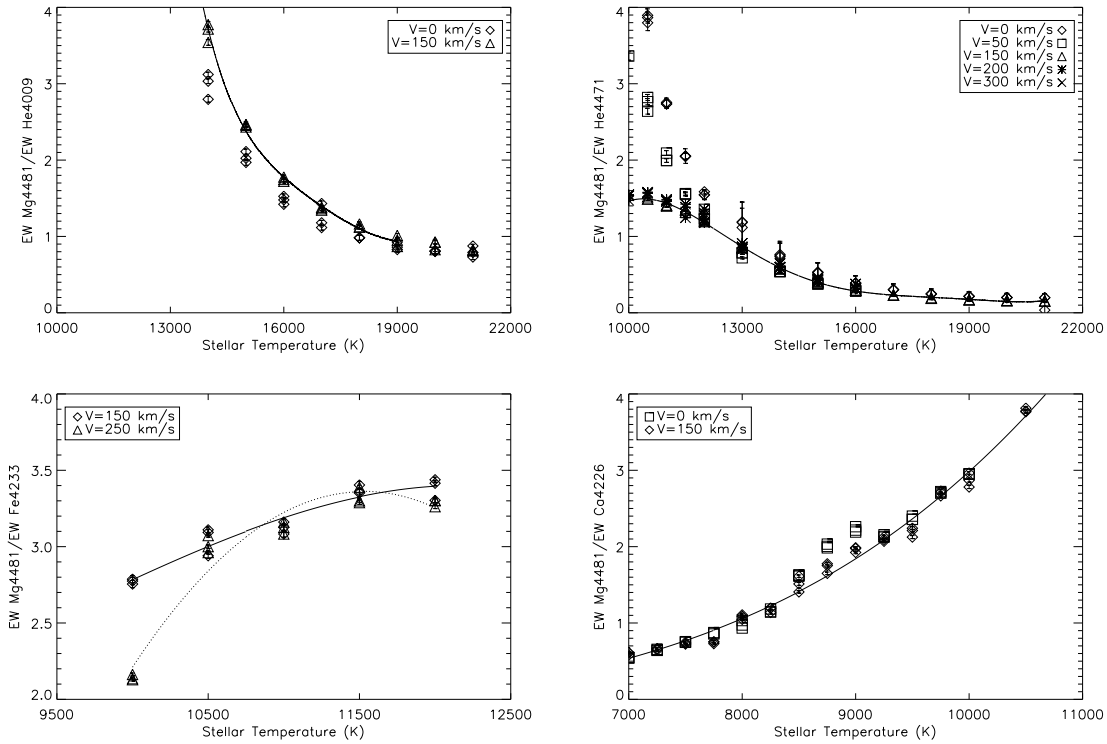

Fig. 2.— (a) The relation between model ratios of EW Mg II λ 4481/EW He I λ 4009 and effective temperature. The *solid* curve shows the best fit relation of EW ratio to effective temperature. A given temperature was measured three times to reduce random errors. (b) The relation between EW Mg II λ 4481/EW He I λ 4471 and effective temperature. (c) The relation between EW Mg II λ 4481/EW He I λ 4233 and effective temperature. (d) The relation between EW Mg II λ 4481/EW Ca I λ 4227 and effective temperature.

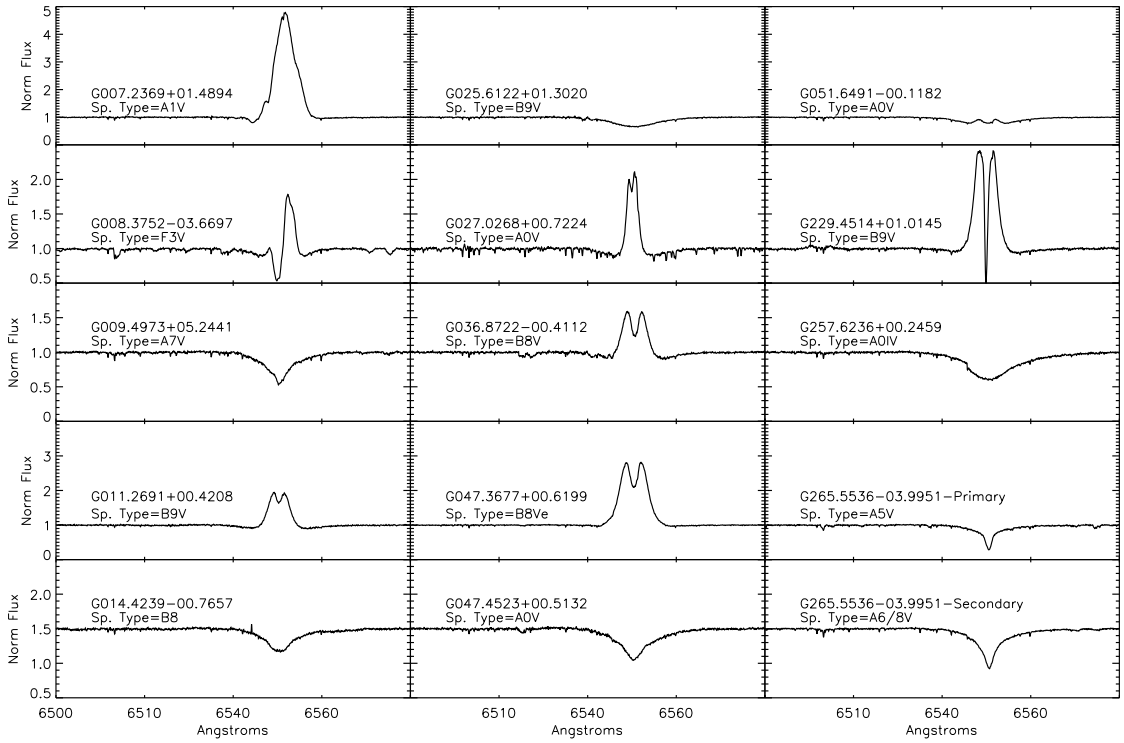

Fig. 3.— Hα profiles of mid-infrared excess stars. The majority of our sources exhibit a double-peaked emission profile.

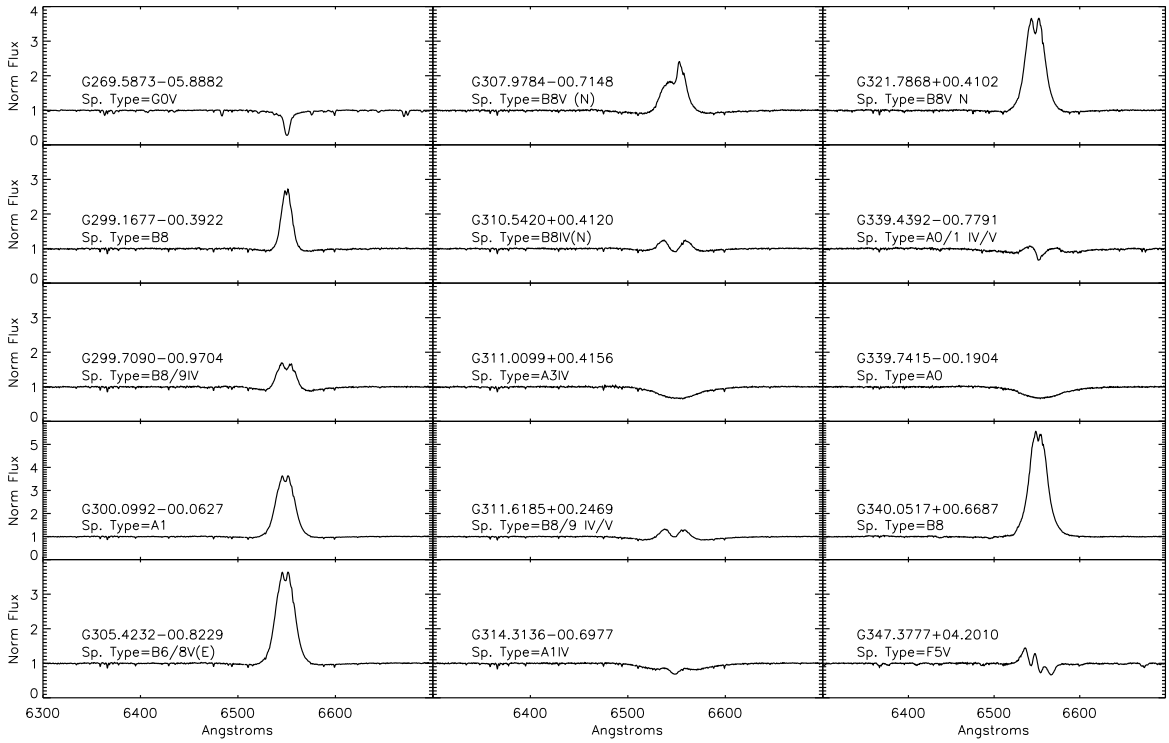

Fig. 4.— Hα profiles of mid-infrared excess stars. The majority of our sources exhibit a double-peaked emission profile.

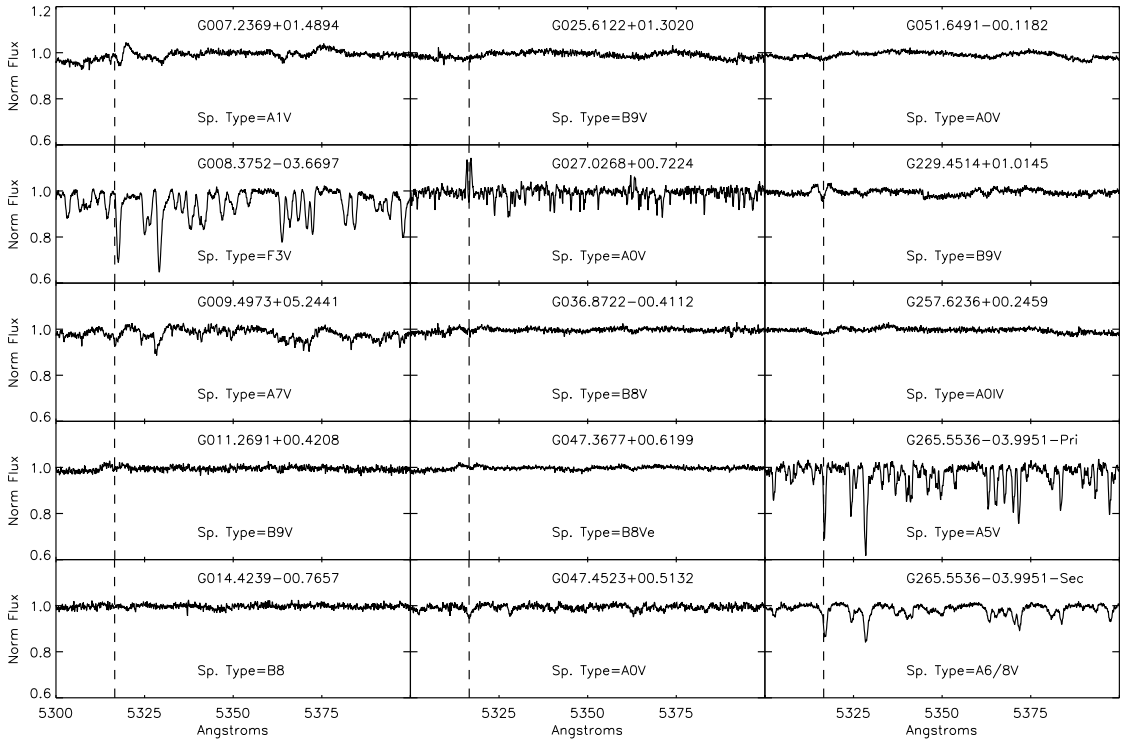

Fig. 5.— Fe II λ 5317Å profiles of mid-infrared excess stars. Fe II is indicated by the *dashed* vertical line. Fe II emission is not very common among our sources.

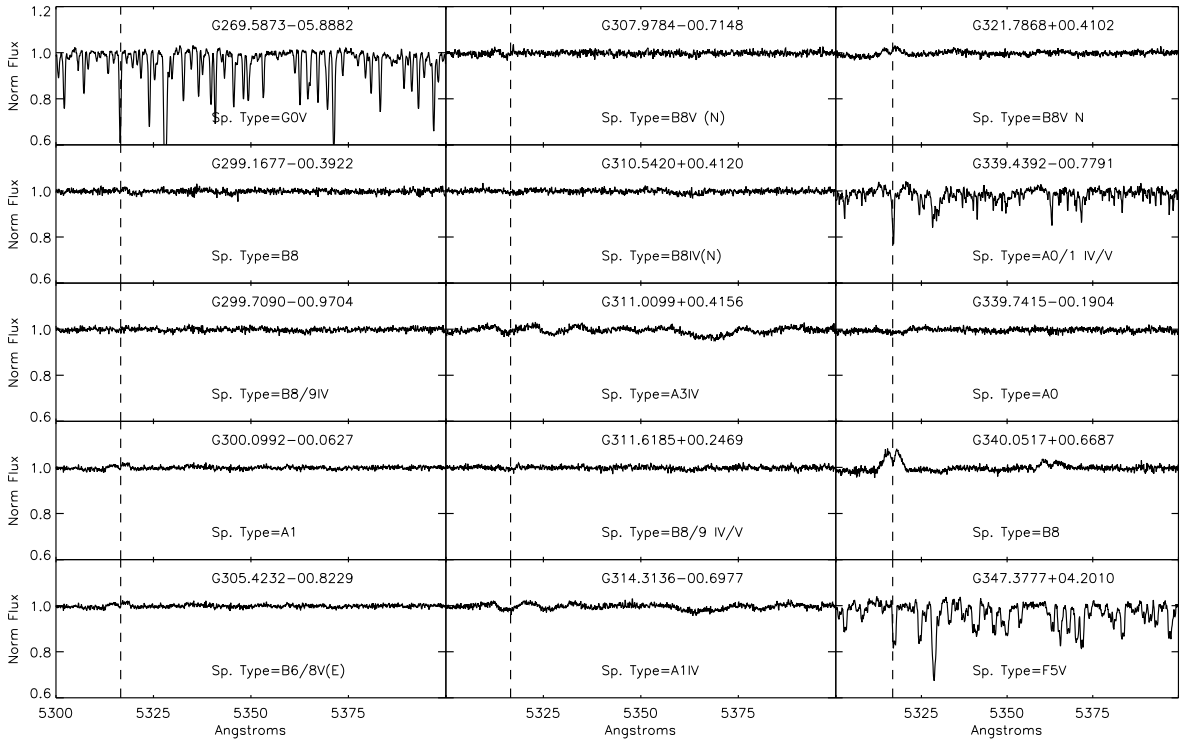

Fig. 6.— Fe II λ 5317Å profiles of mid-infrared excess stars. Fe II is indicated by the *dashed* vertical line. Fe II emission is not very common among our sources.

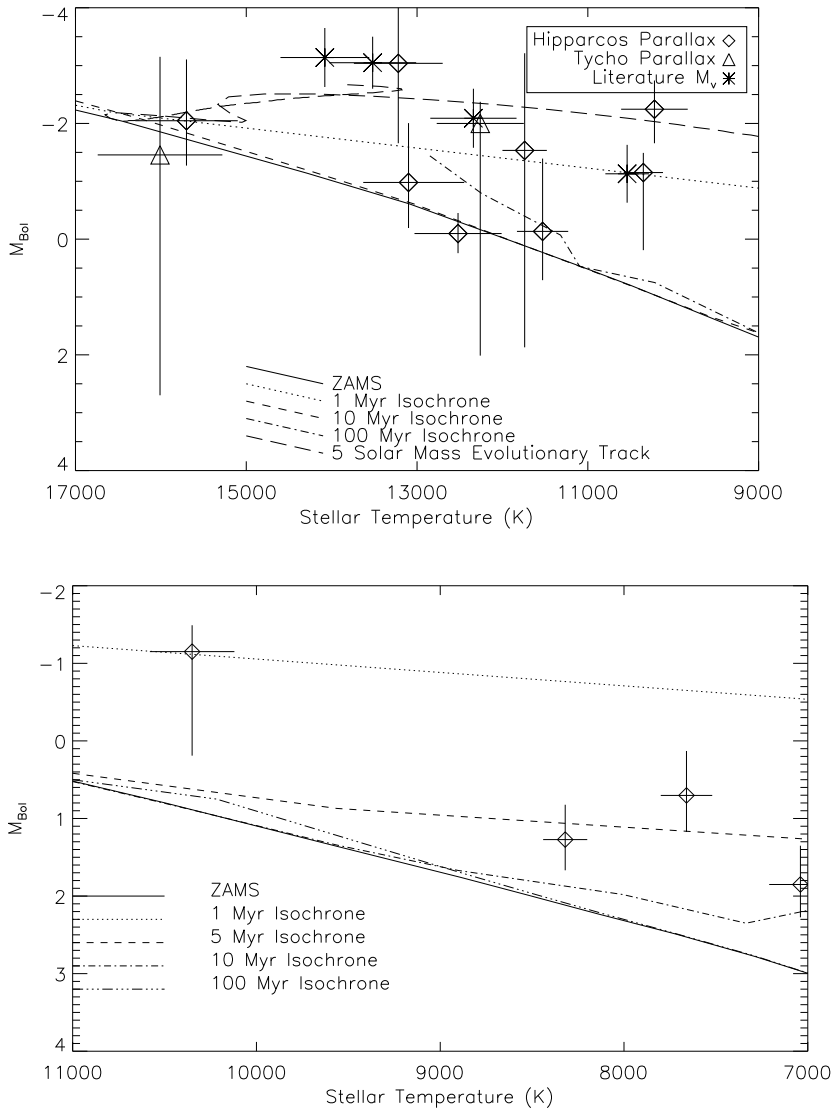

Fig. 7.— (a) HR diagrams for twelve of our target stars overlaid with Siess et al. (2000) stellar evolutionary models for 9000 < T_{eff} < 17000 K. The majority of our stars are above the main-sequence and consistent with 3-5$M_{\odot}$ stars. (b) Siess et al. (2000) models for 7000 < T_{eff} < 11000 K. There is a two star overlap between this diagram and Figure 7a. The three late-type stars are above the main-sequence and consistent with pre-main-sequence stars.

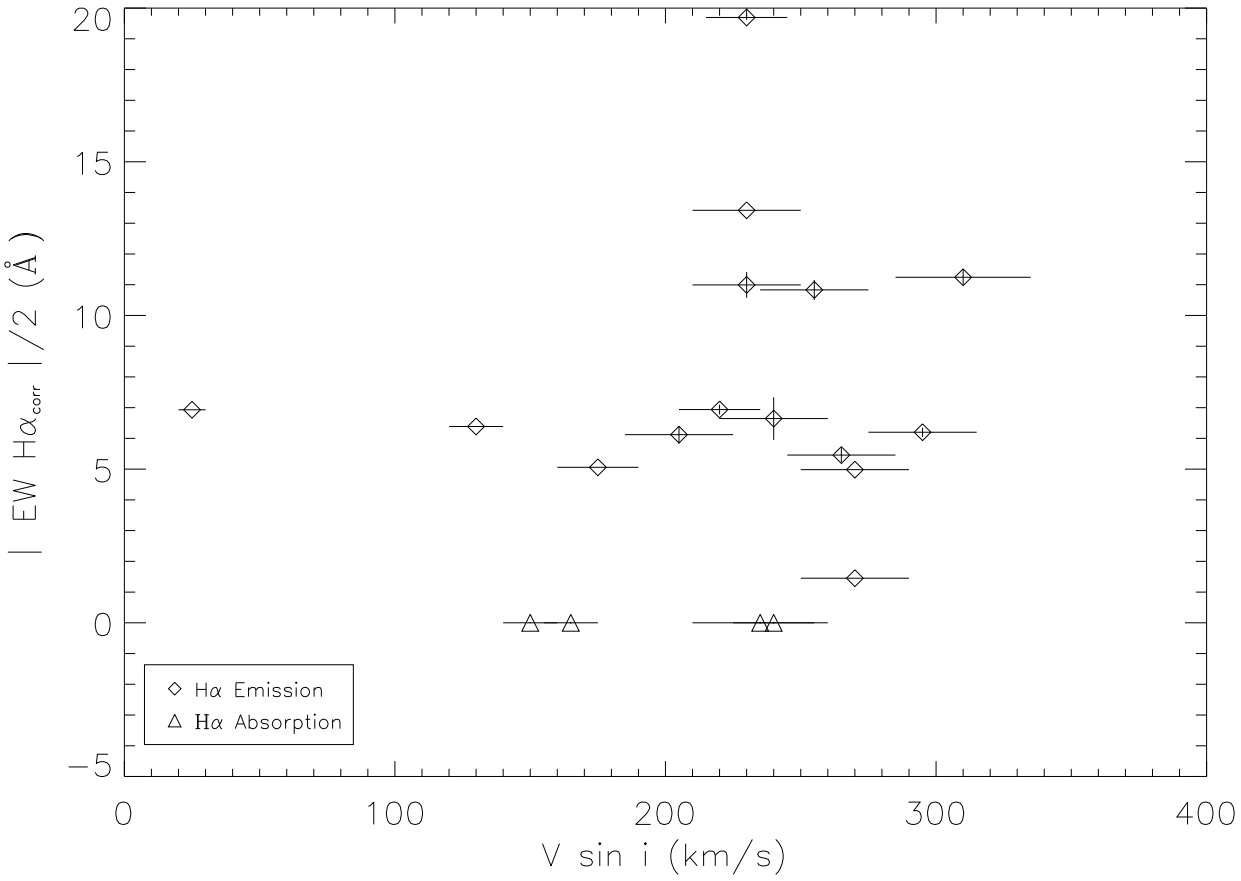

Fig. 8.— Projected rotational velocities vs. Hα half widths of our mid-infrared excess stars. There is no correlation between these two parameters.

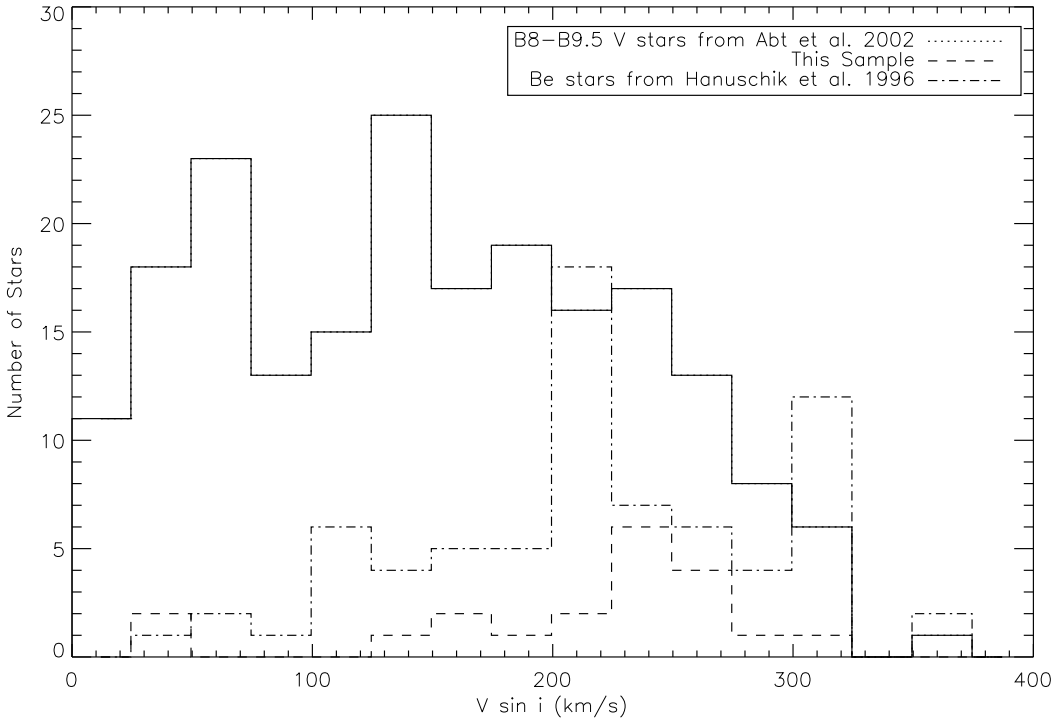

Fig. 9.— A comparison of projected rotational velocities of B8-9.5 V stars from Abt et al. (2002), classical Be stars from Hanuschik et al. (1996), and our GLIMPSE sample. Utilizing a KS test we find that there is no significant probability that our sources are part of either parent population, $< 1\%$ for the Abt et al. (2002) sample and 8% for the Hanuschik et al. (1996) sample.

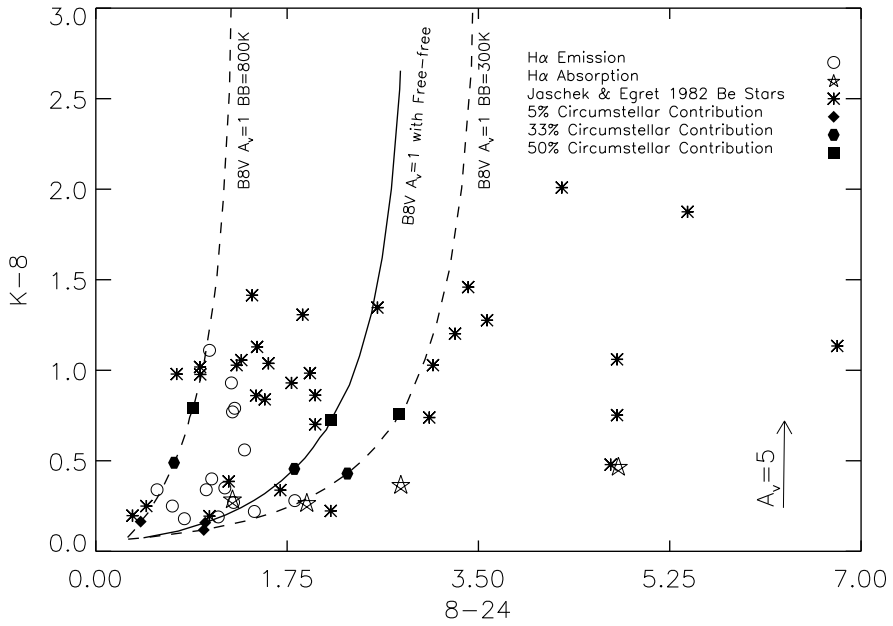

Fig. 10.— An 8-24 μm vs. K-8 μm color-color plot of our objects (open symbols) and classical Be stars (asterisks). Classical Be stars are those from Zhang et al. (2004). MSX A band and IRAS 25 μm (from Zhang et al. 2005) were utilized as 8 μm and 24 μm measurements respectively. The arrow shows the reddening vector for A_V=5.0. The *solid* curve denotes a B8V main-sequence with A_V=1.0 and increasing contribution of free-free flux at 8 μm. The solid symbols denote 5%, 33%, and 50% circumstellar contributions to the total flux at 8 μm. The *dashed* curves denote a B8V main-sequence star with A_V=1.0 and increasing contributions from an 800K and 300K blackbody circumstellar component. This plot shows that excess emission owing to free-free can be distinguished from cool dust (< 300K) in this color-color space, but free-free and hot dust are indistinguishable.

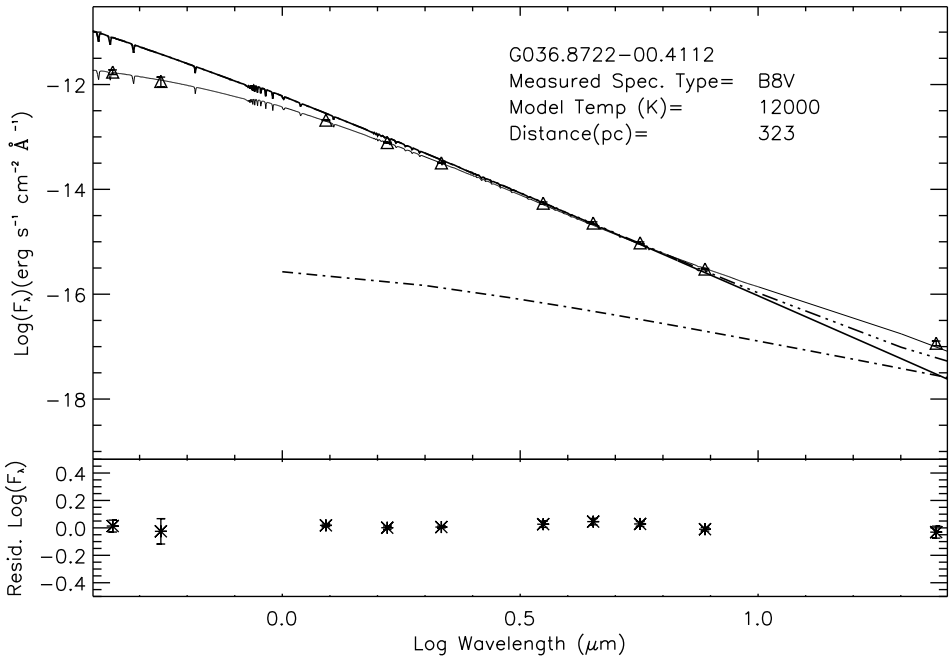

Fig. 11.— Spectral energy distribution of one of our target stars, G036.8722-00.4112. The thick *solid* line is the distance normalized stellar model. The thin *solid* line is the stellar model with extinction and circumstellar blackbody component from Uzpen et al. (2007). The *dash-dot* curve is the modeled free-free component normalized using the Hα flux. The *dash-dot-dot-dot* is the sum of the stellar model with the free-free component. The free-free component is not sufficient to explain the measured excess at 24 μm. The residuals are for the stellar model with circumstellar blackbody component.

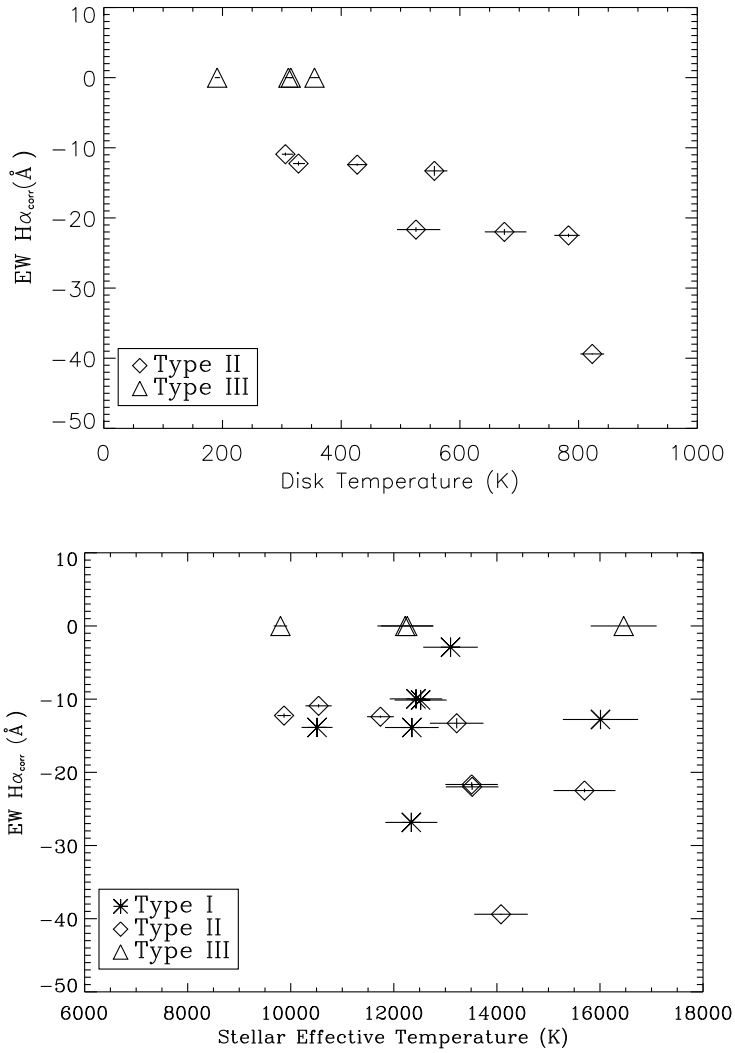

Fig. 12.— (a) Disk temperature vs. Hα equivalent width. There is a strong correlation between these two parameters. (b) Stellar temperature and Hα equivalent width. There is no correlation between these two parameters for either Type I or Type II sources.

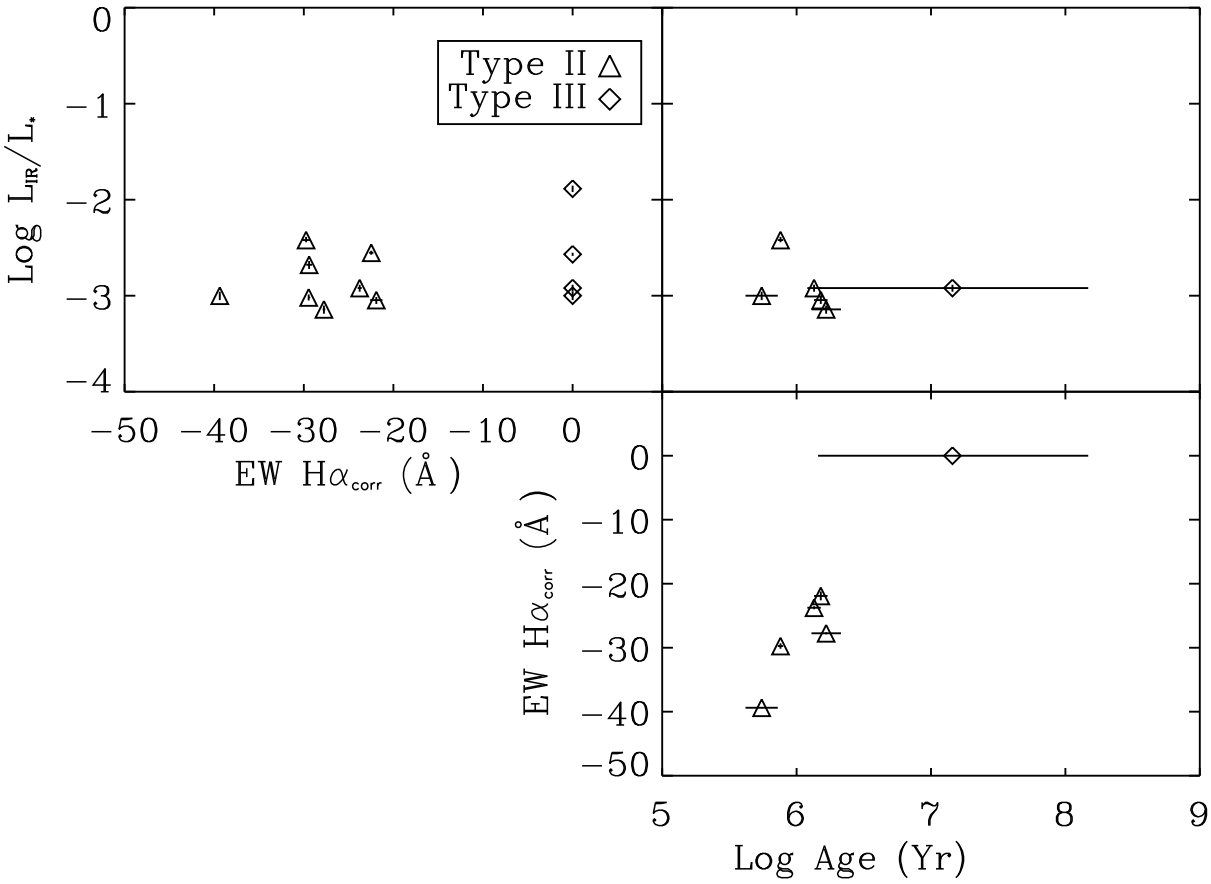

Fig. 13.— An inter-comparison of $\frac{L_{IR}}{L_*}$, age, and Hα equivalent width. Using the younger age, when available, age is correlated with Hα equivalent width with a correlation coefficient of 0.97 indicating $> 99\%$ probability that the two parameters are correlated. for these six stars. Using the older age when available, there is no correlation between age and $\frac{L_{IR}}{L_*}$ or between Hα equivalent width and $\frac{L_{IR}}{L_*}$.

REFERENCES

Abt, H. A., Levato, H., & Grosso, M. 2002, ApJ, 573, 359

Abt, H. A., & Morrell, N. I. 1995, ApJS, 99, 135

Alencar, S. H. P., Melo, C. H. F., Dullemond, C. P., Andersen, J., Batalha, C., Vaz, L. P. R., & Mathieu, R. D. 2003, A&A, 409, 1037

Ashok, N. M., Bhatt, H. C., Kulkarni, P. V., & Joshi, S. C. 1984, MNRAS, 211, 471

Aumann, H. H., Beichman, C. A., Gillett, F. C., de Jong, T., Houck, J. R., Low, F. J., Neugebauer, G., Walker, R. G., & Wesselius, P. R. 1984, ApJ, 278, L23

Backman, D. E., & Paresce, F. 1993, in Protostars and Planets III, ed. E. H. Levy & J. I. Lunine, 1253–1304

Balona, L. A. 2000, in Astronomical Society of the Pacific Conference Series, Vol. 214, IAU Colloq. 175: The Be Phenomenon in Early-Type Stars, ed. M. A. Smith, H. F. Henrichs, & J. Fabregat, 1–58381

Benjamin, R. A., Churchwell, E., Babler, B. L., Bania, T. M., Clemens, D. P., Cohen, M., Dickey, J. M., Indebetouw, R., Jackson, J. M., Kobulnicky, H. A., Lazarian, A., Marston, A. P., Mathis, J. S., Meade, M. R., Seager, S., Stolovy, S. R., Watson, C., Whitney, B. A., Wolff, M. J., & Wolfire, M. G. 2003, PASP, 115, 953

Bernstein, R., Shectman, S. A., Gunnels, S. M., Mochnacki, S., & Athey, A. E. 2003, in Presented at the Society of Photo-Optical Instrumentation Engineers (SPIE) Conference, Vol. 4841, Instrument Design and Performance for Optical/Infrared Groundbased Telescopes. Edited by Iye, Masanori; Moorwood, Alan F. M. Proceedings of the SPIE, Volume 4841, pp. 1694-1704 (2003)., ed. M. Iye & A. F. M. Moorwood, 1694–1704

Bertout, C. 1989, ARA&A, 27, 351

Bjorkman, K. S., Miroshnichenko, A. S., Bjorkman, J. E., Meade, M. R., Babler, B. L., Code, A. D., Anderson, C. M., Fox, G. K., Johnson, J. J., Weitenbeck, A. J., Zellner, N. E. B., & Lupie, O. L. 1998, ApJ, 509, 904

Boehm, T., & Catala, C. 1995, A&A, 301, 155

Brocklehurst, M. 1971, MNRAS, 153, 471

Brosche, P., & Sinachopoulos, D. 1989, Bulletin d'Information du Centre de Donnees Stellaires, 37, 109

Bryden, G., Beichman, C. A., Trilling, D. E., Rieke, G. H., Holmes, E. K., Lawler, S. M., Stapelfeldt, K. R., Werner, M. W., Gautier, T. N., Blaylock, M., Gordon, K. D., Stansberry, J. A., & Su, K. Y. L. 2006, ApJ, 636, 1098

Carroll, J. A. 1933, MNRAS, 93, 478

Chen, C. H., Jura, M., Gordon, K. D., & Blaylock, M. 2005, ApJ, 623, 493

Cidale, L., Zorec, J., & Tringaniello, L. 2001, A&A, 368, 160

Cox, A. N. 2000, Allen's astrophysical quantities (Allen's astrophysical quantities, 4th ed. Publisher: New York: AIP Press; Springer, 2000. Editedy by Arthur N. Cox. ISBN: 0387987460)

Cutispoto, G., Pastori, L., Pasquini, L., de Medeiros, J. R., Tagliaferri, G., & Andersen, J. 2002, A&A, 384, 491

Cutispoto, G., Tagliaferri, G., de Medeiros, J. R., Pastori, L., Pasquini, L., & Andersen, J. 2003, A&A, 397, 987

Dachs, J., Hanuschik, R., Kaiser, D., Ballereau, D., & Bouchet, P. 1986, A&AS, 63, 87

Dachs, J., Kiehling, R., & Engels, D. 1988, A&A, 194, 167

Decin, G., Dominik, C., Waters, L. B. F. M., & Waelkens, C. 2003, ApJ, 598, 636

Egan, M. P., Price, S. D., Kraemer, K. E., Mizuno, D. R., Carey, S. J., Wright, C. O., Engelke, C. W., Cohen, M., & Gugliotti, M. G. 2003, VizieR Online Data Catalog, 5114, 0

Finkenzeller, U. 1985, A&A, 151, 340

Finkenzeller, U., & Mundt, R. 1984, A&AS, 55, 109

Gehrz, R. D., Hackwell, J. A., & Jones, T. W. 1974, ApJ, 191, 675

Grady, C. A., Perez, M. R., Talavera, A., Bjorkman, K. S., de Winter, D., The, P.-S., Molster, F. J., van den Ancker, M. E., Sitko, M. L., Morrison, N. D., Beaver, M. L., McCollum, B., & Castelaz, M. W. 1996, A&AS, 120, 157

Gray, D. F. 1992, The Observation and Analysis of Stellar Photospheres (The Observation and Analysis of Stellar Photospheres, by David F. Gray, pp. 470. ISBN 0521408687. Cambridge, UK: Cambridge University Press, June 1992.)

Gursky, H. 1972, ApJ, 175, L141+

Halbedel, E. M. 1996, PASP, 108, 833

Hamdy, M. A., Elazm, M. S. A., & Saad, S. M. 1991, Ap&SS, 186, 161

Hanuschik, R. W., Hummel, W., Sutorius, E., Dietle, O., & Thimm, G. 1996, A&AS, 116, 309

Hartmann, L., Kenyon, S. J., & Calvet, N. 1993, ApJ, 407, 219

Herbig, G. H. 1960, ApJS, 4, 337

Hernández, J., Briceño, C., Calvet, N., Hartmann, L., Muzerolle, J., & Quintero, A. 2006, ApJ, 652, 472

Hernández, J., Calvet, N., Briceño, C., Hartmann, L., & Berlind, P. 2004, AJ, 127, 1682

Hernandez, J., Hartmann, L., Megeath, T., Gutermuth, R., Muzerolle, J., Calvet, N., Vivas, A. K., Briceno, C., Allen, L., Stauffer, J., Young, E., & Fazio, G. 2007, ArXiv Astrophysics e-prints

Hillenbrand, L. A., Strom, S. E., Vrba, F. J., & Keene, J. 1992, ApJ, 397, 613

Israel, F. P., & Kennicutt, R. C. 1980, Astrophys. Lett., 21, 1

Jaschek, C., & Jaschek, M. 1992, A&AS, 95, 535

Jaschek, M., & Egret, D. 1982, in IAU Symposium, Vol. 98, Be Stars, ed. M. Jaschek & H.-G. Groth, 261–+

Jaschek, M., Jaschek, C., Hubert-Delplace, A.-M., & Hubert, H. 1980, A&AS, 42, 103

Jura, M. 1999, ApJ, 515, 706

Karzas, W. J., & Latter, R. 1961, ApJS, 6, 167

Kessler-Silacci, J., Augereau, J.-C., Dullemond, C. P., Geers, V., Lahuis, F., Evans, II, N. J., van Dishoeck, E. F., Blake, G. A., Boogert, A. C. A., Brown, J., Jørgensen, J. K., Knez, C., & Pontoppidan, K. M. 2006, ApJ, 639, 275

Kozok, J. R. 1985, A&AS, 62, 7

Kurucz, R. L. 1993, SYNTHE spectrum synthesis programs and line data (Kurucz CD-ROM, Cambridge, MA: Smithsonian Astrophysical Observatory, —c1993, December 4, 1993)

Lagrange, A.-M., Backman, D. E., & Artymowicz, P. 2000, Protostars and Planets IV, 639

Levenhagen, R. S., & Leister, N. V. 2004, AJ, 127, 1176

Mannings, V., & Sargent, A. I. 1997, ApJ, 490, 792

Manoj, P., Bhatt, H. C., Maheswar, G., & Muneer, S. 2006, ApJ, 653, 657

Manoj, P., Maheswar, G., & Bhatt, H. C. 2002, MNRAS, 334, 419

Manset, N., Bastien, P., & Bertout, C. 2005, AJ, 129, 480

McSwain, M. V., & Gies, D. R. 2005, ApJS, 161, 118

Meyer, M. R., Hillenbrand, L. A., Backman, D. E., Beckwith, S. V. W., Bouwman, J., Brooke, T. Y., Carpenter, J. M., Cohen, M., Gorti, U., Henning, T., Hines, D. C., Hollenbach, D., Kim, J. S., Lunine, J., Malhotra, R., Mamajek, E. E., Metchev, S., Moro-Martin, A., Morris, P., Najita, J., Padgett, D. L., Rodmann, J., Silverstone, M. D., Soderblom, D. R., Stauffer, J. R., Stobie, E. B., Strom, S. E., Watson, D. M., Weidenschilling, S. J., Wolf, S., Young, E., Engelbracht, C. W., Gordon, K. D., Misselt, K., Morrison, J., Muzerolle, J., & Su, K. 2004, ApJS, 154, 422

Monet, D. G. 1998, in Bulletin of the American Astronomical Society, Vol. 30, Bulletin of the American Astronomical Society, 1427–+

Monet, D. G., Levine, S. E., Canzian, B., Ables, H. D., Bird, A. R., Dahn, C. C., Guetter, H. H., Harris, H. C., Henden, A. A., Leggett, S. K., Levison, H. F., Luginbuhl, C. B., Martini, J., Monet, A. K. B., Munn, J. A., Pier, J. R., Rhodes, A. R., Riepe, B., Sell, S., Stone, R. C., Vrba, F. J., Walker, R. L., Westerhout, G., Brucato, R. J., Reid, I. N., Schoening, W., Hartley, M., Read, M. A., & Tritton, S. B. 2003, AJ, 125, 984

Monnier, J. D., Millan-Gabet, R., Billmeier, R., Akeson, R. L., Wallace, D., Berger, J.-P., Calvet, N., D'Alessio, P., Danchi, W. C., Hartmann, L., Hillenbrand, L. A., Kuchner, M., Rajagopal, J., Traub, W. A., Tuthill, P. G., Boden, A., Booth, A., Colavita, M., Gathright, J., Hrynevych, M., Le Mignant, D., Ligon, R., Neyman, C., Swain, M., Thompson, R., Vasisht, G., Wizinowich, P., Beichman, C., Beletic, J., Creech-Eakman, M., Koresko, C., Sargent, A., Shao, M., & van Belle, G. 2005, ApJ, 624, 832

Mora, A., Merín, B., Solano, E., Montesinos, B., de Winter, D., Eiroa, C., Ferlet, R., Grady, C. A., Davies, J. K., Miranda, L. F., Oudmaijer, R. D., Palacios, J., Quirrenbach, A., Harris, A. W., Rauer, H., Cameron, A., Deeg, H. J., Garzón, F., Penny, A., Schneider, J., Tsapras, Y., & Wesselius, P. R. 2001, A&A, 378, 116

Munari, U., Sordo, R., Castelli, F., & Zwitter, T. 2005, A&A, 442, 1127

Oudmaijer, R. D., van der Veen, W. E. C. J., Waters, L. B. F. M., Trams, N. R., Waelkens, C., & Engelsman, E. 1992, A&AS, 96, 625

Pogodin, M. A. 1994, A&A, 282, 141

Porter, J. M., & Rivinius, T. 2003, PASP, 115, 1153

Royer, F. 2005, Memorie della Societa Astronomica Italiana Supplement, 8, 124

Royer, F., Gerbaldi, M., Faraggiana, R., & Gómez, A. E. 2002a, A&A, 381, 105

Royer, F., Grenier, S., Baylac, M.-O., Gómez, A. E., & Zorec, J. 2002b, A&A, 393, 897

Schütz, O., Meeus, G., & Sterzik, M. F. 2005, A&A, 431, 165

Seidensticker, K. J. 1989, A&AS, 79, 61

Shu, F. H., Adams, F. C., & Lizano, S. 1987, ARA&A, 25, 23

Sicilia-Aguilar, A., Hartmann, L., Calvet, N., Megeath, S. T., Muzerolle, J., Allen, L., D'Alessio, P., Merín, B., Stauffer, J., Young, E., & Lada, C. 2006a, ApJ, 638, 897

Sicilia-Aguilar, A., Hartmann, L. W., Fürész, G., Henning, T., Dullemond, C., & Brandner, W. 2006b, AJ, 132, 2135

Siegler, N., Muzerolle, J., Young, E. T., Rieke, G. H., Mamajek, E. E., Trilling, D. E., Gorlova, N., & Su, K. Y. L. 2007, ApJ, 654, 580

Siess, L., Dufour, E., & Forestini, M. 2000, A&A, 358, 593

Skinner, S. L., Brown, A., & Stewart, R. T. 1993, ApJS, 87, 217

Slettebak, A., Collins, II, G. W., Parkinson, T. D., Boyce, P. B., & White, N. M. 1975, ApJS, 29, 137

Spangler, C., Sargent, A. I., Silverstone, M. D., Becklin, E. E., & Zuckerman, B. 2001, ApJ, 555, 932

Spitzer, L. 1978, Physical processes in the interstellar medium (New York Wiley-Interscience, 1978. 333 p.)

Strom, K. M., Strom, S. E., Edwards, S., Cabrit, S., & Skrutskie, M. F. 1989, AJ, 97, 1451

Strom, S. E. 1972, PASP, 84, 745

Struve, O. 1931, ApJ, 73, 94

The, P. S., de Winter, D., & Perez, M. R. 1994, A&AS, 104, 315

Tucker, W. 1975, Radiation processes in astrophysics (Cambridge, Mass., MIT Press, 1975. 320 p.)

Uzpen, B., Kobulnicky, H. A., Monson, A. J., Pierce, M. J., Clemens, D. P., Backman, D. E., Meade, M. R., Babler, B. L., Indebetouw, R., Whitney, B. A., Watson, C., Wolfire, M. G., Benjamin, R. A., Bracker, S., Bania, T. M., Cohen, M., Cyganowski, C. J., Devine, K. E., Heitsch, F., Jackson, J. M., Mathis, J. S., Mercer, E. P., Povich, M. S., Rho, J., Robitaille, T. P., Sewilo, M., Stolovy, S. R., Watson, D. F., Wolff, M. J., & Churchwell, E. 2007, ApJ, 658, 1264

Viallefond, F., Donas, J., & Goss, W. M. 1983, A&A, 119, 185

Viallefond, F., & Goss, W. M. 1986, A&A, 154, 357

Viallefond, F., Goss, W. M., van der Hulst, J. M., & Crane, P. C. 1986, A&AS, 64, 237

Vieira, S. L. A., Corradi, W. J. B., Alencar, S. H. P., Mendes, L. T. S., Torres, C. A. O., Quast, G. R., Guimarães, M. M., & da Silva, L. 2003, AJ, 126, 2971

Vink, J. S., Drew, J. E., Harries, T. J., & Oudmaijer, R. D. 2002, MNRAS, 337, 356

Voges, W., Aschenbach, B., Boller, T., Brauninger, H., Briel, U., Burkert, W., Dennerl, K., Englhauser, J., Gruber, R., Haberl, F., Hartner, G., Hasinger, G., Pfeffermann, E., Pietsch, W., Predehl, P., Schmitt, J., Trumper, J., & Zimmermann, U. 2000, VizieR Online Data Catalog, 9029, 0

Wade, G. A., Drouin, D., Bagnulo, S., Landstreet, J. D., Mason, E., Silvester, J., Alecian, E., Böhm, T., Bouret, J.-C., Catala, C., & Donati, J.-F. 2005, A&A, 442, L31

Walker, H. J., Volk, K., Wainscoat, R. J., Schwartz, D. E., & Cohen, M. 1989, AJ, 98, 2163

Waters, L. B. F. M., & Waelkens, C. 1998, ARA&A, 36, 233

Werner, M. W., Roellig, T. L., Low, F. J., Rieke, G. H., Rieke, M., Hoffmann, W. F., Young, E., Houck, J. R., Brandl, B., Fazio, G. G., Hora, J. L., Gehrz, R. D., Helou, G., Soifer, B. T., Stauffer, J., Keene, J., Eisenhardt, P., Gallagher, D., Gautier, T. N., Irace, W., Lawrence, C. R., Simmons, L., Van Cleve, J. E., Jura, M., Wright, E. L., & Cruikshank, D. P. 2004, ApJS, 154, 1

Westin, T. N. G. 1985, A&AS, 60, 99

Wright, C. O., Egan, M. P., Kraemer, K. E., & Price, S. D. 2003, AJ, 125, 359

Yudin, R. V. 2001, A&A, 368, 912

Zhang, P., Chen, P. S., & He, J. H. 2004, New Astronomy, 9, 509

Zhang, P., Chen, P. S., & Yang, H. T. 2005, New Astronomy, 10, 325

Zuckerman, B. 2001, ARA&A, 39, 549

This preprint was prepared with the AAS LaTeX macros v5.2.